

5. SECONDARY BEAM

5.1 Secondary Beam Layout

The layout of elements in the secondary beam as shown in Table 5.1.1.

Table 5.1.1
Layout of Elements in the Secondary Beam

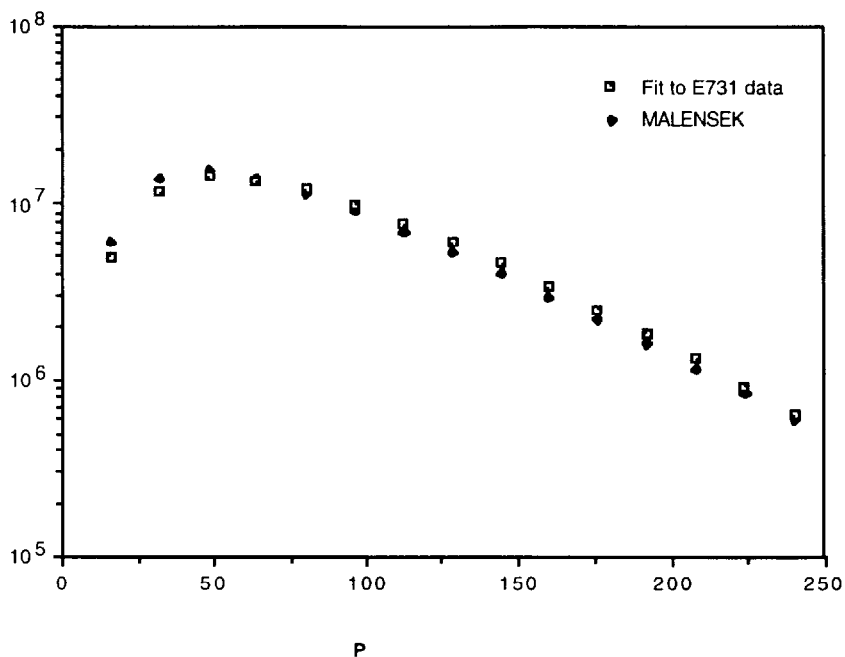
z (m) upstrm edge	z(m) dnstrm edge	x (cm) half- width	y (cm) half- width	B (kg)	Name
-0.15	+0.15				target
0.58	4.39	2.35	+2.29 to -4.06	5.0	NM2S1 -Early sweeper
7.10	11.66	2.66	+1.92 to -1.54		primary passive dump
12.27	17.76	2.83	1.69	23.0	NM2S2-hyperon sweeper
18.21	19.39				Be and Pb filters
19.50	21.50	0.54 0.60	0.58 0.66		Upstream/primary two-hole fixed collimator
21.90	27.69	4.91	2.00	20.0	NM2S3 (m sweeper2)
30.47	36.53	4.96	4.96	13.0	NM2S4 (spin rotator dipole)
39.00	41.00				slab collimator
42.76	45.81				beam stop
46.24	47.76				horiz. "jaw" variable collimator
49.24	50.76				vert. "jaw" variable collimator
85.00	88.00	2.12 2.20	2.12 2.20		Downstream/defining two-hole fixed collimator
90.27	92.10	11.56	4.45	≤18.0	NM3S (final sweeper)
123.4	125.2				regenerator
168.5	171.5			3.5	NM3AN (analysis magnet)
184.0	184.2				trigger scintillator hodoscope
186.0	186.5				CsI

Half width in x and y planes refer to the inner aperature of the magnets.

5.2 Flux Calculations

The K_L fluxes are calculated using the Malensek parameterization³² assuming K_L flux is the average of the charged kaon fluxes. The Malensek fit agrees reasonably well with the E731 momentum spectrum³³ as shown in Fig. 5.2.1. The K_L flux calculated is about 30% higher than observed in the E731 vacuum beam. We use the E731 K_L estimate of 1×10^7 K_L per 1×10^{12} incident protons to normalize the KTeV predictions.³⁴ This is reliable since the E731 target, targetting angle, absorbers, and solid angle is essentially identical to KTeV.

Fig. 5.2.1 Comparison of E731 data and Malensek parametrization of K_L momentum spectrum



The neutron fluxes are more difficult to predict. We have used information from previous E731 data on the rate of interactions in two detectors placed directly in the neutral beam (the regenerator veto counters

³² A.J. Malensek, Fermilab FN-341.

³³ J.R. Patterson, Determination of $\text{Re}(\epsilon'/\epsilon)$ by the Simultaneous Detection of the Four $K_{L,S} \rightarrow \pi\pi$ Decay Modes, Dec.1990, U. Chicago dissertation.

³⁴ L. K. Gibbons, A Precise Measurement of CP-Violation and other Kaon Decay Parameters, August 1993, University of Chicago dissertation.

and back-anti photon veto) which give $n/K_L = 2 \pm 1$ for the E832 vacuum beam. This ratio is based on subtracting the rate due to the known K_L flux and correcting for detector efficiencies. Some of these efficiencies are momentum dependent due to energy thresholds in the detectors. We measure the K_L momentum spectrum in previous experiments and use a fit to neutron production measurements³⁵ to get the shapes of the momentum spectra. As a check, we have used the same neutron fit and the measured K_L to predict $n/K_L = 0.5$ while a similar independent estimate found $n/K_L = 1$.³⁶ The implications of this uncertainty are discussed more in section 5.11.

The photon fluxes were estimated using a fit of data from an FNAL photon beam³⁷. The lambda flux was calculated using fits to data³⁸. The neutral particle fluxes for 1×10^{12} incident 800 GeV protons on Be target with a 4.8 mrad targetting angle is shown in Fig. 5.2.2 before any filtering. Photons dominate the neutral particle spectrum. To reduce the photon component we insert lead a filter to reduce the photon flux to an acceptable level. We also add Be filters to improve the n/K_L ratio. In addition we target at 4.8 mrad to improve the n/K_L ratio (Fig. 5.2.3). The results below include these filters. Note these rates are for the "standard" beam of 0.25 msteradians per beam. This is a conservatively small size motivated by the E832 beam specifications. A larger beam might be possible, particularly for E799II. As discussed further in section 5.8 we plan to build collimator inserts which would also allow us to run with either 1.5 or 2.0 x the standard solid angle of 0.25 msteradians per beam subject to backgrounds and radiation damage of the CsI.

³⁵ Edwards et al, Phys. Rev. D18, 76(1978) modified with a pt dependence from Engler et al, Nucl. Phys. B84, 70(1975).

³⁶ private communication, R. Bernstein.

³⁷ private communication, A.J. Malensek.

³⁸ Pondrom et al, Phy. Reports, 122,67,(1985)

Figure 5.2.2 KTeV neutral particle fluxes at production before filters for 1 E12 incident 800 GeV protons (4.8 mr targetting angle)

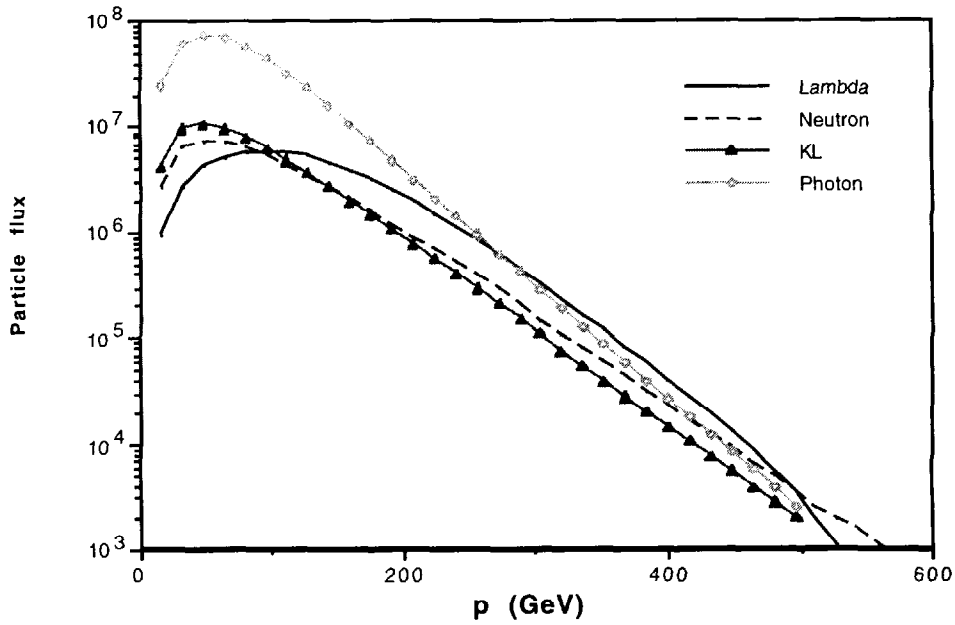


Figure 5.2.3 KL flux (no filters) per 1E12 incident 800 GeV protons and KL/neutron ratio vs. vertical targetting angle (Note: KTeV range = 4.0 to 5.5 mr, "nominal" = 4.8 mr)

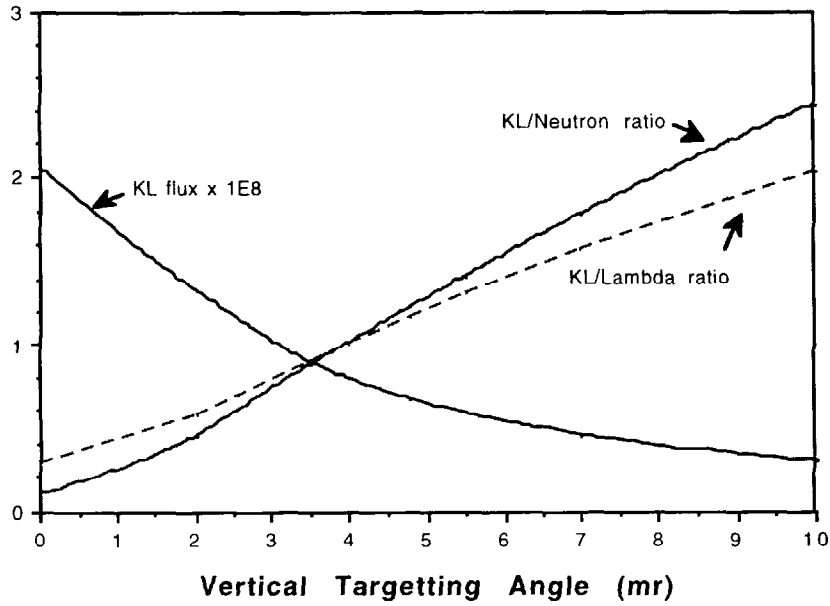


Table 5.1.2
Neutral Fluxes

	E832 vacuum	E832 regenerator	E799 both beams
incident protons	3.5×10^{12}	3.5×10^{12}	5×10^{12}
K_L	3.5×10^7	1.4×10^7	2.9×10^8
neutron	7.0×10^7	2.2×10^7	1.1×10^9
lambda	1.7×10^4	5.2×10^3	2.6×10^5
filters	3" Pb + 20" Be	3"Pb + 38" Be	3" Pb
K_L transmission	.19	.076	.55
n transmission	.10	.031	.54

Neutral fluxes at $z = 90$ m from the target including filters per spill (solid angle = 0.25 mster. per beam). The transmission includes the effect of absorption and scattering from the filters.

5.3 Justifications for Beam Stability Requirements

In order that the measurement to e'/e in E832 not be compromised by systematic effects, E832's e'/e analysis requires the sizes and positions of the two neutral beams be stable to 0.5 mm, that the areas be equal (to 1%), and that the kaon momentum spectra be equal (to 0.1%).³⁹ In the final analysis, after the results from the two beams are used optimally and after the Monte Carlo has been appropriately tuned to fit the data, these systematic problems should disappear. The goal is to keep the beam-related systematic problems well below the level of sensitivity of the experiment. The requirements are based primarily on the E731 analysis.⁴⁰ Additionally, there are analytic/numerical calculations—primarily relating to variations in the momentum spectrum. Finally there are various results based on a series of runs with a small Monte Carlo program to address specific issues such as beam geometry and 2π acceptances. The sensitivity of e'/e to neutral beam motion was estimated by comparison of different E731 data sets and the corresponding Monte Carlo correction sets. Because of the target and collimator alignment instabilities, the beam areas varied from about 2% to 10%. For each data set the Monte Carlo collimator positions are adjusted to match the beam shape for that data set. Therefore, by analyzing different data sets with non-corresponding Monte Carlo corrections for the e'/e analysis, we

³⁹ private communication, B. Hsiung.

⁴⁰ Ibid, B. Hsiung.

are able to estimate the change in ϵ'/ϵ induced by a changed in beam position at the regenerator. The result is

$$\frac{d\epsilon'/\epsilon}{dX_{reg}} = 3 \times 10^{-4} / \text{cm}$$

where X_{reg} is the neutral beam position at the regenerator in the plane of the two beams.⁴¹

A similar analysis was done with regard to the momentum equality of the two beams. The result is

$$\frac{d\epsilon'/\epsilon}{d\langle p_{sec} \rangle} < 3 \times 10^{-3} / \text{GeV}.$$

Using the variation of the momentum spectrum with production angle of 0.7 GeV/mrad, this corresponds to $\frac{d\epsilon'/\epsilon}{d\theta_x} < 2 \times 10^{-3} / \text{mrad}$. One may also estimate⁴² this dependence with a Monte Carlo with the KTeV geometry and using the Malensek momentum dependence. From these, one may estimate the sensitivity of ϵ'/ϵ to the production angle as it is effected through the momentum spectrum. The spectrometer acceptance averaged over z and p is Ω .

The result is

$$\begin{aligned} \frac{d(\epsilon'/\epsilon)}{d\theta_x} &= \frac{d(\epsilon'/\epsilon)}{d(\Delta\Omega/\Omega)} \frac{d(\Delta\Omega/\Omega)}{d(\Delta\langle p_{sec} \rangle / \langle p_{sec} \rangle)} \frac{d(\Delta\langle p_{sec} \rangle / \langle p_{sec} \rangle)}{d\theta_x} \\ &= (1/6) \quad (0.34) \quad (0.018/\text{mrad}) \\ &= 1 \times 10^{-3} / \text{mrad}. \end{aligned}$$

which is not in disagreement with the E731 limit quoted above.

The E832 goal is to measure ϵ'/ϵ to at least 1 part in 10^4 . In order to keep errors due to the beam small, our goal is 0.2 parts in 10^4 . To keep the two beam fluxes equal to 1% the horizontal targetting angle must be stable to 0.28 mrad. To keep the mean momentum equal of the two beams equal to 0.1% the horizontal targetting angle must be stable to 28 mrad. To keep the beam momentum equal to 0.1% due to the vertical targetting angle is more

⁴¹ Ibid, B. Hsiung.

⁴² D. Jensen, On the Sensitivity of ϵ'/ϵ to Primary Beam Parameters, Feb. 2, 1994, KTeV memo.

stringent and is about 20 mrad. This is due to the 4.8 mrad vertical targetting angle compared to the 0.8 mrad horizontal angle. These results are obtained from the Monte Carlo using the Malensek momentum dependence. There are geometric tolerances also if the fluxes are to be equal (areas of two beams must be equal). These constraints are discussed in section 5.8.6.

The sensitivity of e'/e to the beam parameters has been propagated by standard error analysis. The term must be added in quadrature and be less than 0.2×10^{-4} .

$$\frac{d(\epsilon'/\epsilon)}{d\langle p_{sec} \rangle} \frac{d\langle p_{sec} \rangle}{d\theta_x} \Delta\theta_x + \frac{d(\epsilon'/\epsilon)}{dX_{reg}} \frac{dX_{reg}}{dx_{beam}} \Delta x_{beam} < 0.2 \times 10^{-4}$$

The primary beam position on target is the x_{beam} term. For our 1mm x 1mm target, the position correlation term is negligible, so only the $\Delta\theta_x$ term contributes.

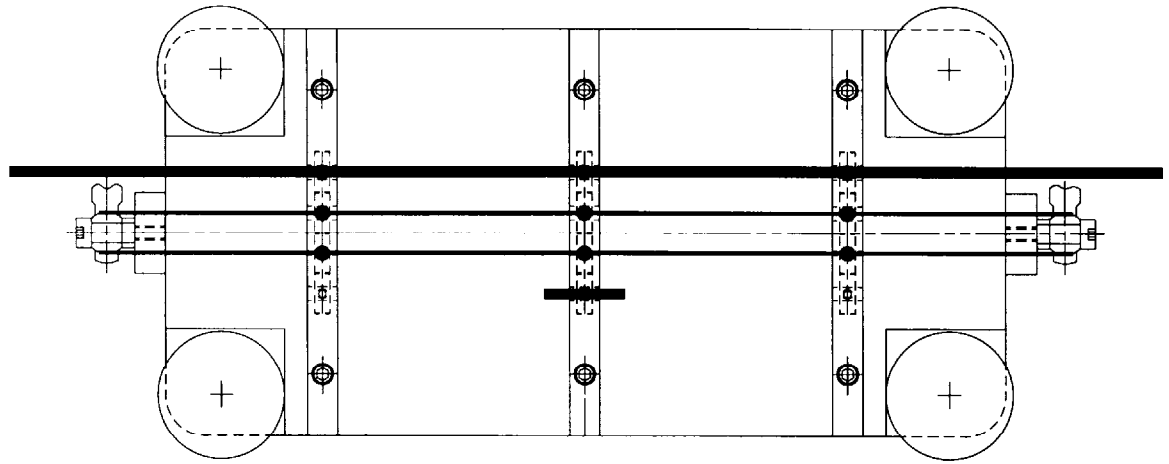
The result is $(1 \times 10^{-3}/\text{GeV})(0.7 \text{ GeV/mrad})(\Delta\theta_x) < 0.2 \times 10^{-4}$ or $\Delta\theta_x < 28$ mrad. Ignoring angle changes, the 2nd term above can be interpreted as target motion. The correlation term $\frac{dX_{reg}}{dx_{beam}}$ is 1.5 so the target stability due to this concern is 0.043 cm. However for good targetting efficiency on the 1 mm x 1mm target we require 0.020 cm positional stability of the primary beam and target.

5.4 Target Design

The KTeV target requirements are discussed in the Design Report⁴³. The material of choice is BeO and the length is 30 cm or about 1 interaction length. Two different cross section size BeO targets are planned, 1mm and 3mm. A thin target is included to use with the collimator alignment scheme discussed in section 5.9. Finally, we will also mount the Be target used in the previous Meson Center experiments for comparison with BeO. These targets will all be mounted in a remotely controlled target holder with a target-out position. A layout of the targets and target holder is shown in Fig. 5.4.1.

⁴³ KTeV Design Report, January 22, 1992, FN-580.

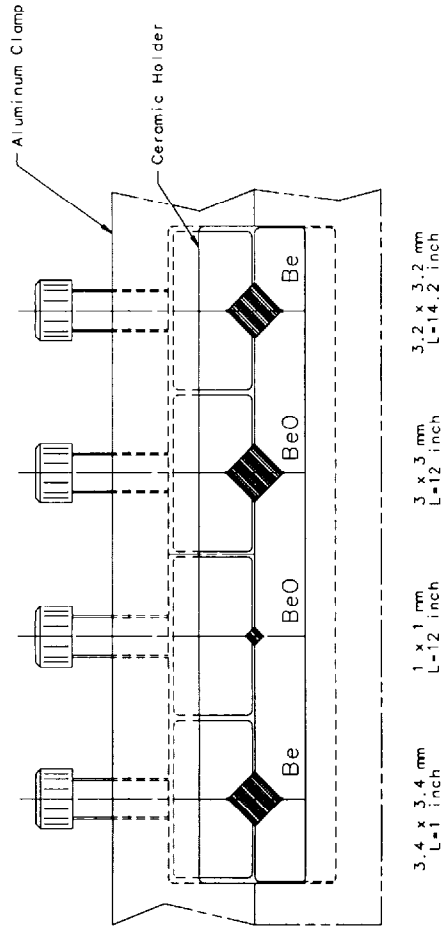
TOP VIEW



Beam Direction



BEAM VIEW LOOKING DOWNSTREAM



Aluminum Clamp

Ceramic Holder

3.4 x 3.4 mm
L=1 inch

1 x 1 mm
L=12 inch

3 x 3 mm
L=12 inch

3.2 x 3.2 mm
L=14.2 inch

Figure 5.4.1 Targets

The targets must be aligned with respect to the neutral beam line precisely (200 microns).

The heating issues associated with a 1 mm square target are summarized in Table 5.4.1. The heating calculations were done for 1 E13 incident 900 GeV protons per pulse with a 20 second spill length and a 60 second cycle time. Beryllium was evaluated as well as Beryllium Oxide.

Table 5.4.1
Summary of Heating Calculations

Cooling Method	Beryllium		Beryllium Oxide	
	T(min)	T(max)	T(min)	T(max)
Forced Convection	310 K	360 K	310 K	420 K
Natural Convection	320 K	560 K	320 K	880 K
Radiation Only	700 K	1000 K	720 K	1350 K

1mm target diameter, beam sigma= 0.22 mm

Forced convection is helium gas flowing at 4 meters/sec. and maintaining a temperature no higher than 100 F (310 K). Natural convection is air at a temperature no higher than 100 F. An enclosed target cave will probably have higher temperatures because the air will be "stagnant". T(min) is the temperature just before the beam spill; T(max) is the temperature at the end of the spill. T(min) and T(max) are given after reaching steady state.

Beryllium:

Emissivity = 0.25
 Density = 1.85 g/cc
 Specific Heat = 0.436 cal/g-C
 Melting Temperature = 1550 K

Beryllium Oxide:

Emissivity = 0.25
 Density = 2.85 g/cc
 Specific Heat = 0.24 cal/g-C
 Melting Temperature = 2840 K

The results for a slightly larger beam size and a 3 mm target size are given in Table 5.4.2.

Table 5.4.2
Summary of Heating Calculations

Cooling Method	Beryllium		Beryllium Oxide	
	T(min)	T(max)	T(min)	T(max)
Forced Convection	310 K	350 K	310 K	440 K
Natural Convection	420 K	510 K	560 K	820 K
Radiation Only	710 K	780 K	860 K	1080 K

3 mm target diameter, beam sigma= 0.35 mm

5.5 Primary Beam Dump Background Elimination

For reference the E731 dump is shown in Fig. 5.5.1; the radial separation was $R = 4.86$ cm for the neutral channel to the proton beam dump center. The spot size of the primary beam at the dump face was about 1 cm full-width for 99% containment. The dump face was located at $z=8.98$ m from the target center. The horizontal target angle of 4.8 mrad gives 4.32 cm separation at the dump. The target sweepers gave an additional 2.23 cm vertical separation at the dump face.

The background from the dump can be estimated from target-out data. From E731 the 2π target-out trigger rates for charged and neutral are 0.006 of target-in, the ET (total lead-glass energy above 28 GeV) target-out rate is 0.03 of the target-in rate.

The KTeV version with the dump face at $z= 7.1$ m and an 4.8 mrad vertical targetting angle is shown in Fig. 4.1.4. The radial separation and the spot size are similar to E731 [$R=3.4$ cm and spot size of 99% containment for < 0.6 (1.5) cm vertical (horizontal) full-width]. The radial separation of the projected proton beam at the face of the hyperon magnet is $R = 8.1$ cm. The length of the dump is much longer for KTeV and the downstream portion (hyperon magnet) is magnetized so we do not anticipate significant backgrounds from the dumping of the primary beam in the neutral channel.

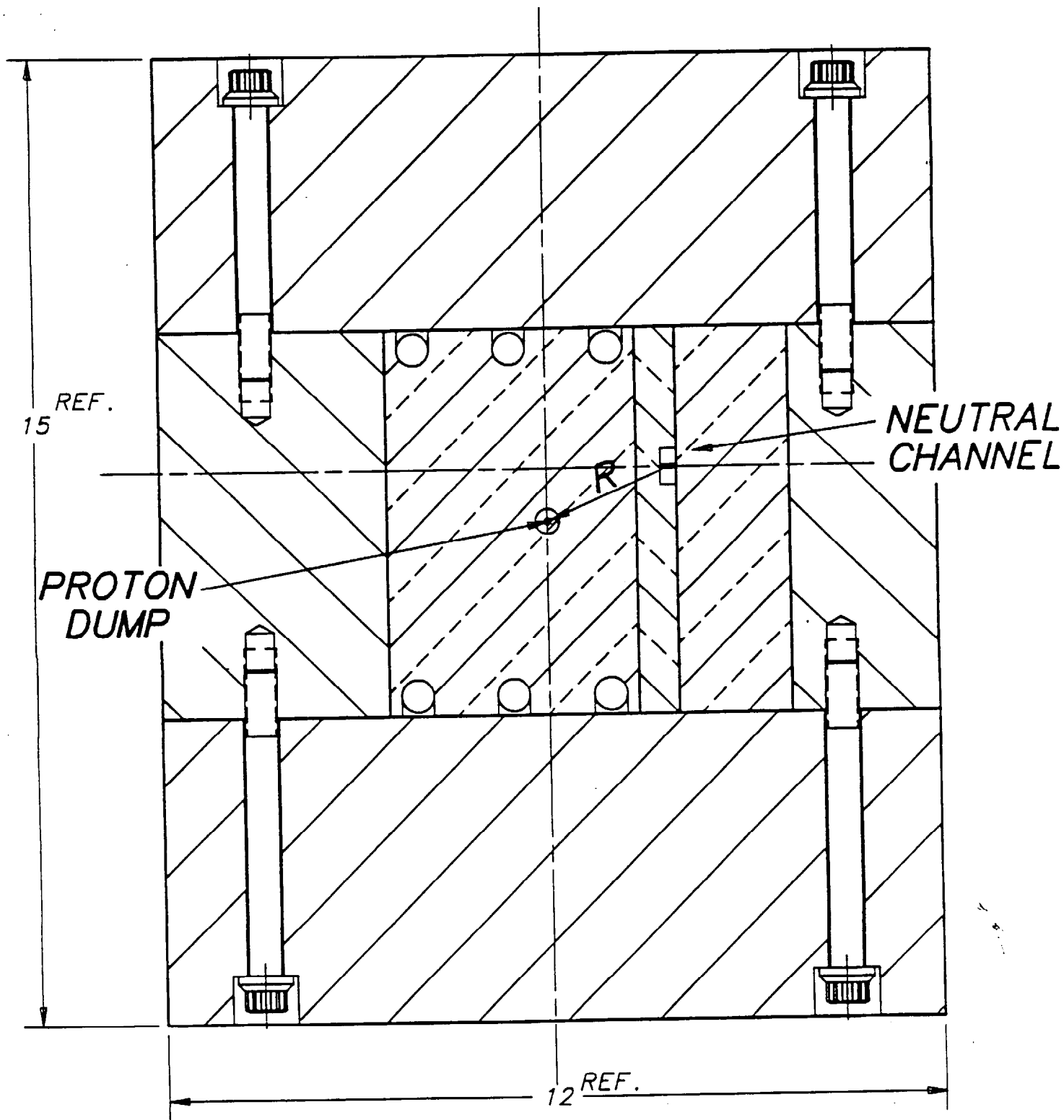


Fig. 5.5.1 E-731 Proton Dump $R=4.86\text{cm}$

5.6 Elimination of Charged Particles from the Neutral Channel

Fig 5.6.1 and 5.6.2 show the magnetic field vs distance from the target along the beam for MC and KTeV (not including the final dweeper at 90 m). Experience from sweeper studies in the MC beamline (E731) shows only small trigger rate effects in varying sweeper currents. For example reducing the most upstream MC sweeper by 2/3 increased the muon rate by 40% while two track trigger (with muon veto) and ET (total lead-glass above 28 GeV) rates only increased by about 5%. Switching off the MC sweeper at $z=30$ m increased the two track trigger rate by 12%. Switching off the MC sweeper at $z=57$ m increased the two track trigger rate by 2%. For the KTeV beamline we will have additional magnetic sweeping relative to the MC beamline (1.7 times more field integral) due to the enhanced muon sweeping system. Even a 800 GeV charged particle leaving the target initially parallel to the neutral channel will strike the inner walls of the hyperon magnet almost 2 m from the downstream end of the 5.5 m long magnet.

Fig. 5.6.1 E731 magnetic sweeping
Integral $B \cdot dl = 203 \text{ kg-m}$

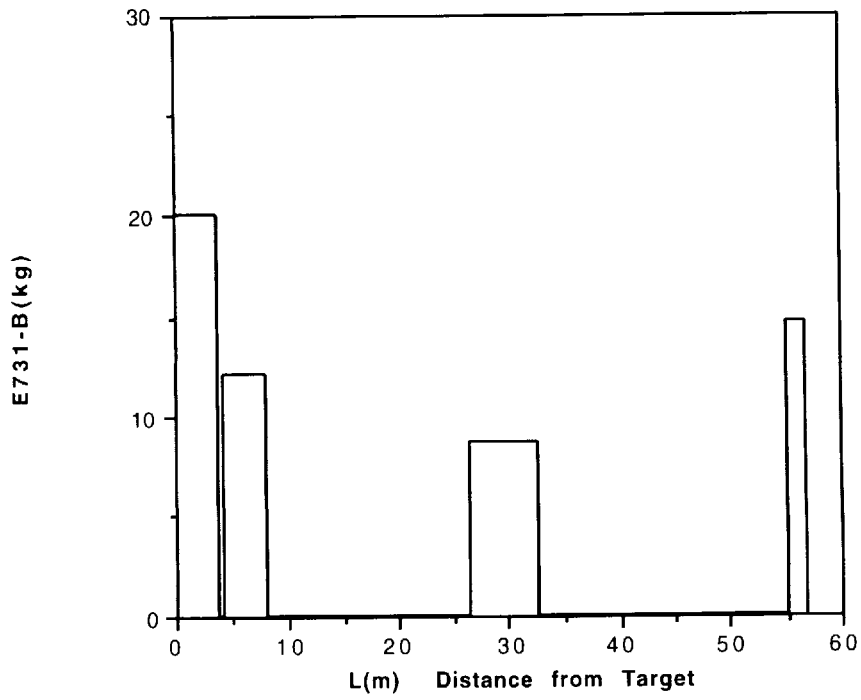
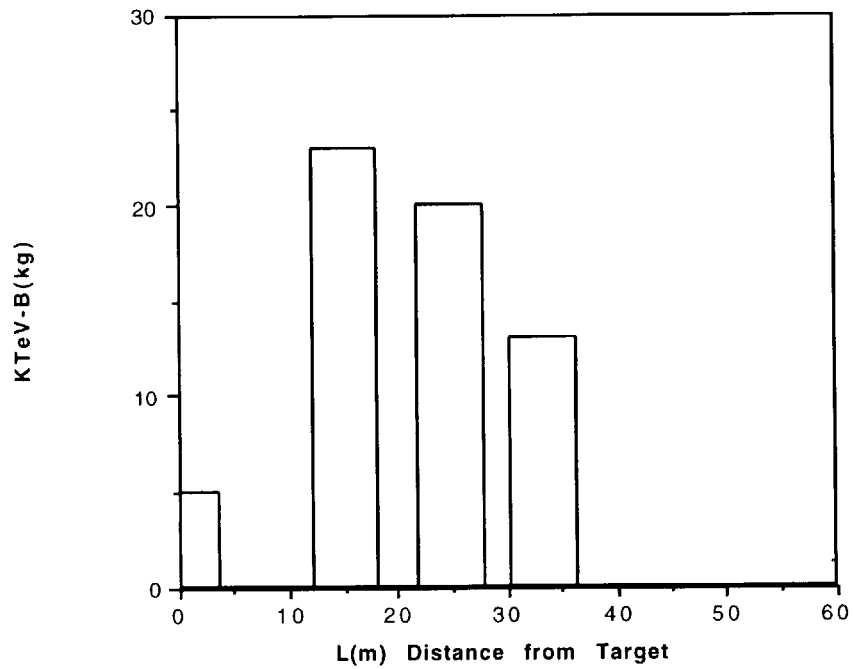


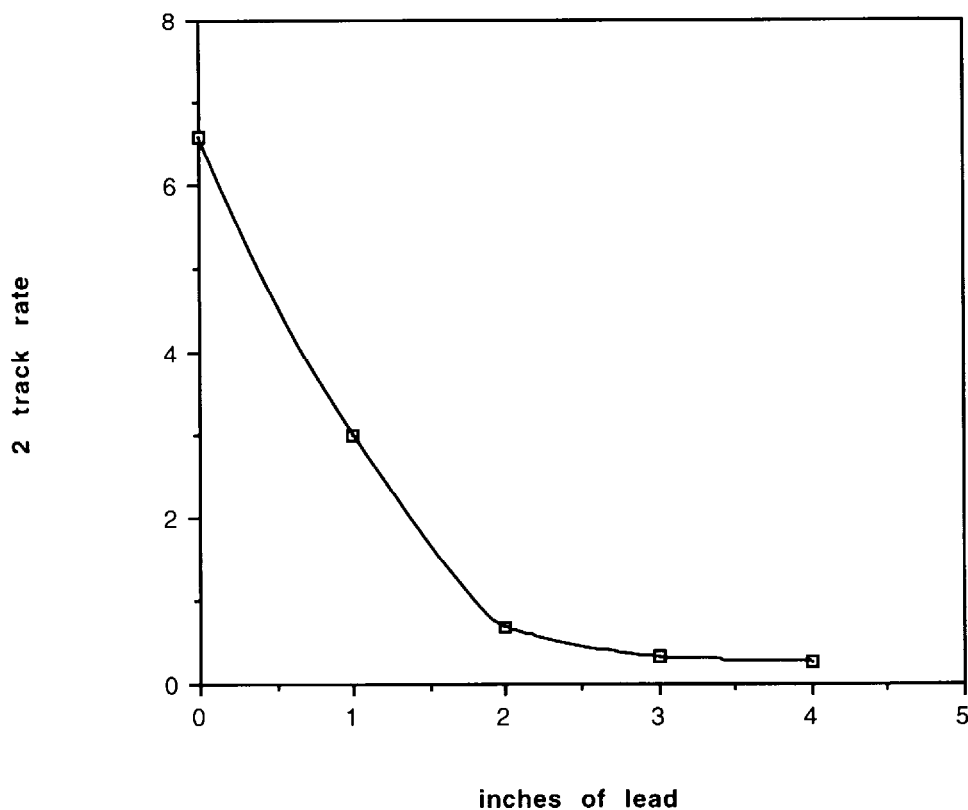
Fig. 5.6.2 KTeV magnetic sweeping
Integral $B \cdot dl = 340 \text{ kg-m}$



5.7 Filter System—Photon Elimination and K_L/n Enhancement

In all of the past experiments using the MC beamline a lead filter was inserted to reduce the photon flux in the neutral beam. Fig. 5.7.1 shows data from E731 logbooks; the charged two track trigger rate with a "veto-on-hits" in the muon detector versus thickness of lead in the neutral beam. We have chosen 3" as the optimal thickness for the lead photon filter.

Fig. 5.7.1 E731 two-track trigger rate versus thickness of lead filter



For E799I the only filter used was the lead discussed above. For E731 a "common" absorber of 20" of Be was placed in both neutral beams and a "movable-shadow" absorber of 18" of Be was placed in the same neutral beam as the regenerator. The various filter transmissions are given in Table 5.1.2. For example, the n/K_L in the E731 regenerator beam is reduced by 2.5 relative to using no Be filters (E799I), while the K_L flux is reduced by 5.1. The interaction length for high energy neutrons (K_L 's) in Be is 40 (55) cm. The interaction length for neutrons (K_L 's) in lead is 16.8 (14.8) cm.⁴⁴ Fig. 5.7.2 shows the engineering design of absorber trays and movers.

⁴⁴ A. Gsponer et al, Phys. Rev. Lett. 42, 9 (1979) and T. J. Roberts et al., Nucl. Phys. B159, 56 (1979).

5.8 Collimator System

5.8.1 Design goals

It is crucial that the collimator system prevent beam halo from causing radiation damage to the CsI or introducing background triggers. Simulations indicate that the scattering of beam particles in filters combined with collimator misalignments was a source of beam halo (see section 5.11). The collimator scheme involves a primary collimator ($z=19.5$ to 21.5 m) and a defining collimator ($z=85$ to 88 m). The defining collimator provides the principle definition of the edges of the beam. To obtain sharp edges, it is located as far downstream as possible. Experience in the MC beamline shows that a collimator at $z=85$ to 88 m does not introduce a dominant background source for the experiment. GEANT studies are consistent with this observation. The primary collimator is located as close as possible to the target. There is a filter just upstream of the primary collimator. The function of the primary collimator is to limit the lateral size of the beam at the scattering source. The combination of the primary and defining collimators then defines the maximum deviation of a scattered neutral particle from the beam axis at the z position of the CsI calorimeter. The goal is to constrain all such scattered tracks to lie within the beam holes, missing the calorimeter. The holes in the CsI are 15.0 cm square separated by 30 cm (center to center) in the horizontal plane. The criteria we have adopted is that all scattered rays fall a minimum of 1 cm inside the holes.

The finite target size also has implications on the collimator design. The walls of the collimator are tapered to point to an apex downstream of the target (Fig. 5.8.1), so that no neutral track from the target can strike the inner walls of the collimator. In practice, the difference in taper is significant only for the primary collimator. These design considerations are discussed in more detail KTeV Design Report⁴⁵. The results are listed below. Additional collimator inserts allow for beams with larger solid angle 1.5 and $2.0\times$ the "standard" beam of 0.25 msteradians per beam.

⁴⁵ KTeV Design Report, January 22, 1992.

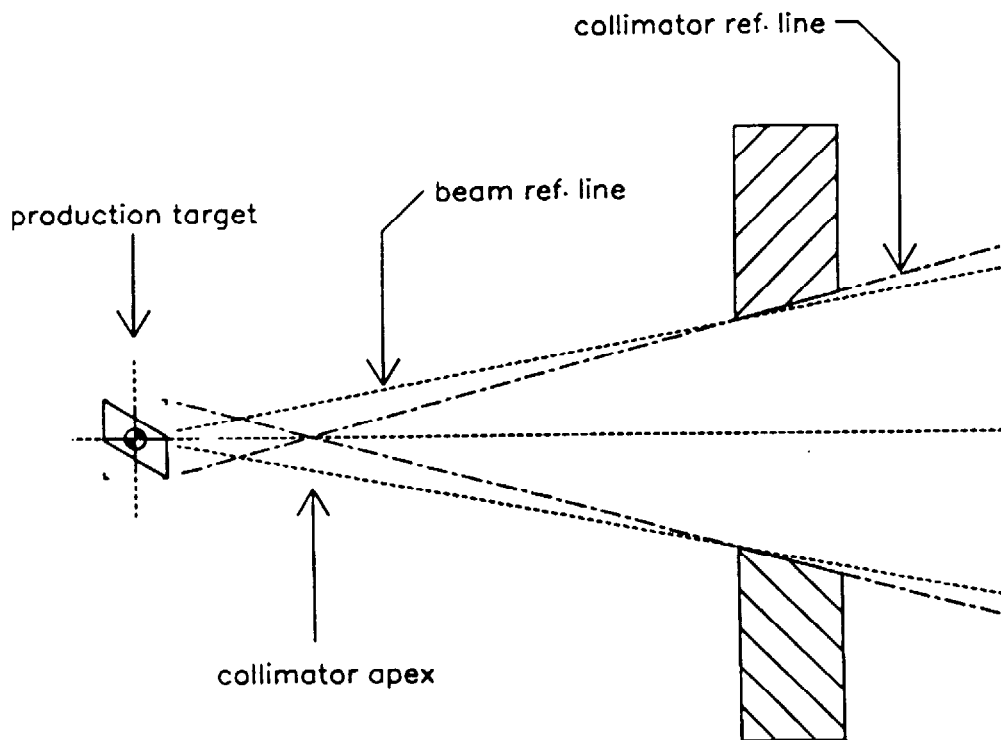


Figure 5.8.1 The walls of the collimator lie on lines that, projected forward, cross at a point called the *collimator apex*. If the target lies entirely upstream of the apex within the cone defined by these lines, then no neutral track emanating from the target can strike the inner walls of the collimator aperture.

The following are used to specify the "standard" beam:

'Target' size 1mm x 1 mm x 30 cm

Beam separation ± 15 cm at CsI (z=186m) center to center

X angular divergence ± 0.250 mrad

Y angular divergence ± 0.250 mrad

Neutral Beam Solid Angle = $4 \times (0.250 \text{ mrad})^2 = 0.250 \mu\text{steradians per beam}$

In addition to the primary and defining collimators there are two other types of collimation; a slab and a pair of variable jaw collimators. The purpose of the slab collimator is to prevent scattered tracks out of one beam from crossing over to the other beam in the plan view. Fig. 5.8.2 illustrates

the principle which is discussed in more detail in the KTeV Design Report⁴⁶. The variable jaw collimators will be used, if needed, to reduce the flux on the defining collimator. Finally, we will have a fast acting beam stop to close completely to block the neutral beam for special studies and radiation safety measurements. We have existing jaw collimators and a beam stop which can be reused with some refurbishments. The slab is a new device. The primary and defining collimator are discussed in more detail in section 5.8.4 and 5.8.5.

5.8.2 System Layout

System layout and apertures for standard beam, aperture sizes are shown below in Table 5.8.2.

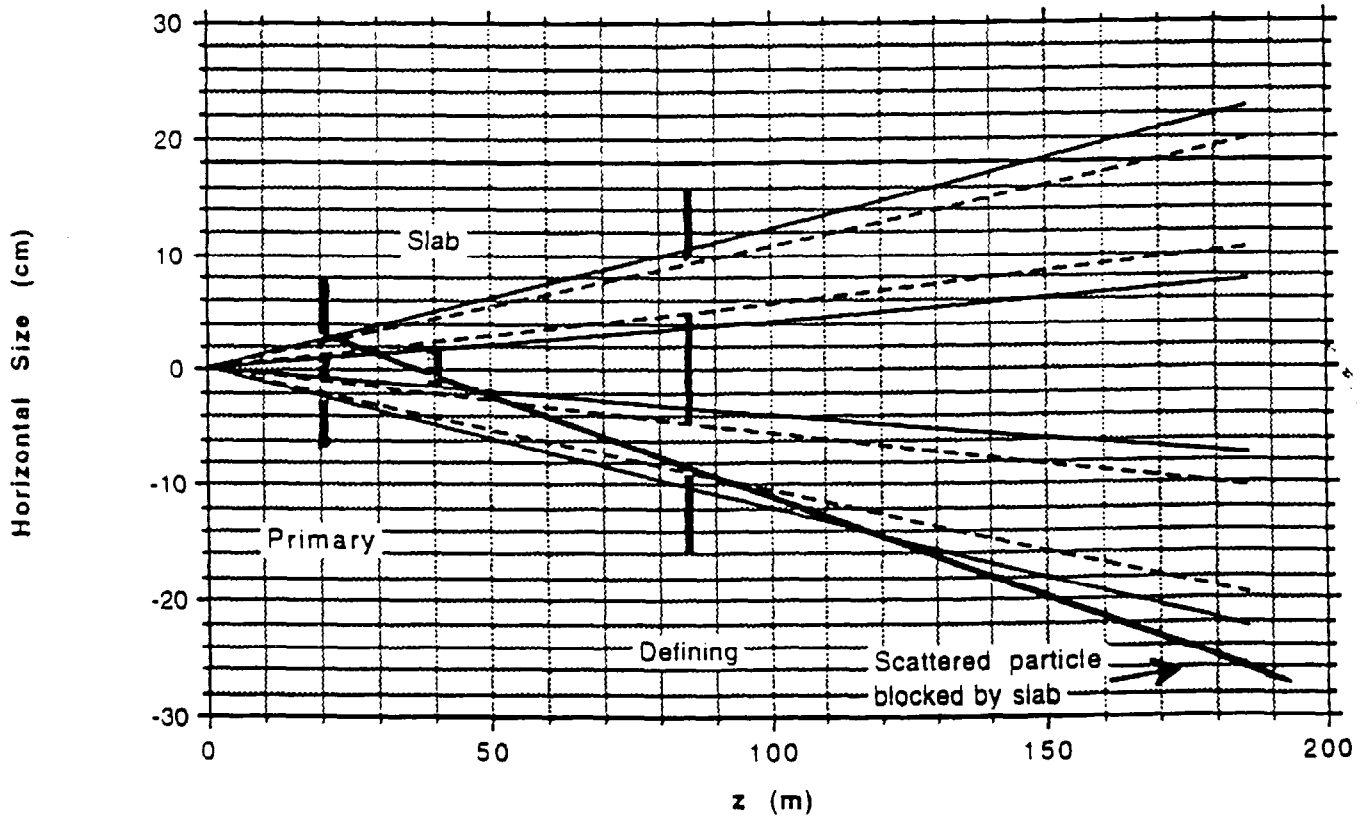
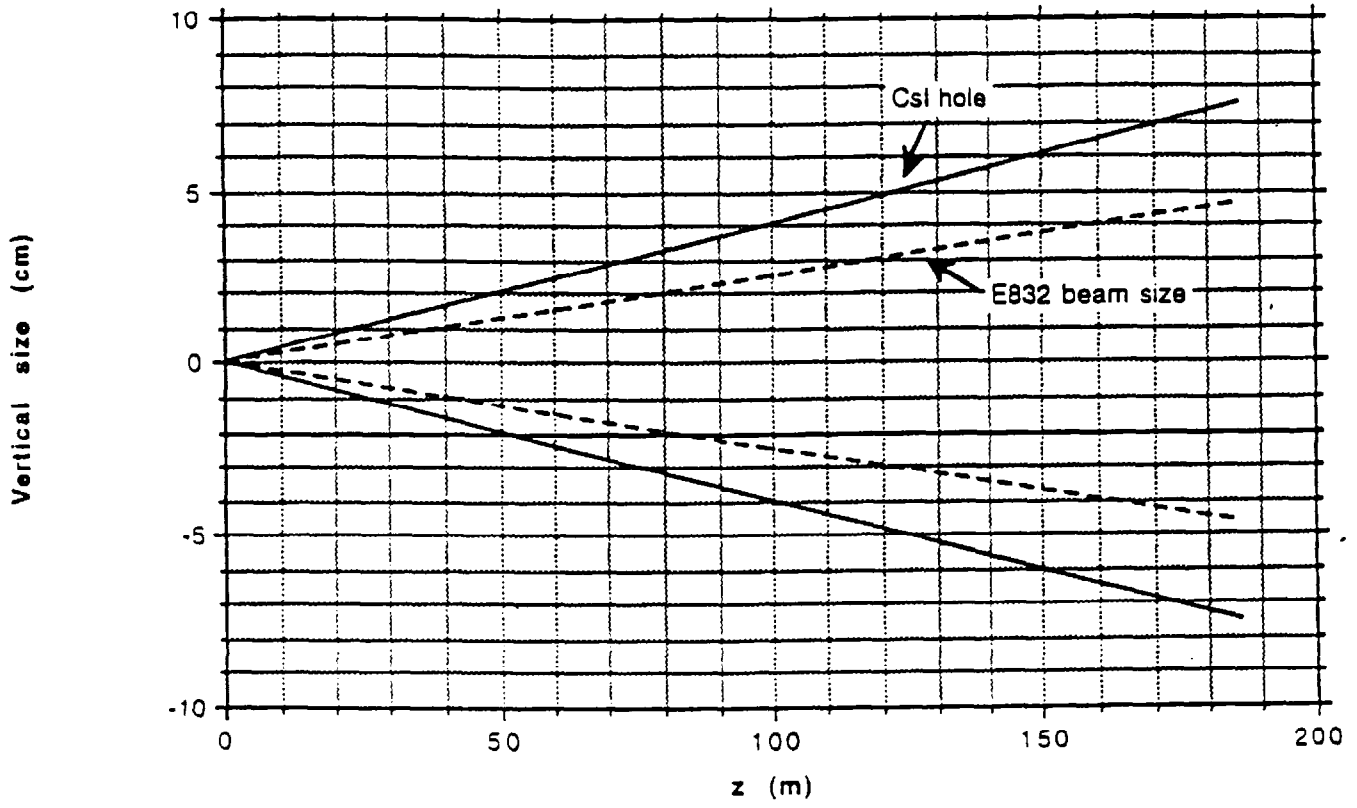
Table 5.8.2
System Layout

Item	X(cm) full-width	Y(cm) full-width	Z(m) location
PC Collimator upstream hole	1.08	1.16	19.5
PC Collimator downstream hole	1.20	1.32	21.5
slab upstream width	2.03		39.0
slab downstream width	2.13		41.0
DC collimator upstream hole	4.24	4.24	85.0
DC collimator downstream hole	4.40	4.40	88.0
Beam size at CsI	9.30	9.30	186.0
Beam hole size at CsI	15.0	15.0	186.0

System layout and apertures for standard beam.

⁴⁶ Ibid, page 74.

Fig. 5.8.2 KTeV Beam Envelope and Collimator Locations



5.8.3 General Considerations of Collimator Outer Dimensions

The outer dimensions of the collimator must be large enough to contain the showers from neutral beam interactions. The neutral flux ($n + K_L$) passing through the CsI beam holes in the highest intensity running for E799II (both beams) is 0.8 to 2.1×10^9 . The range quoted reflects the uncertainty in the n/K_L ratio. Under these conditions the primary collimator ($z=20.5$ m) will be struck with a neutral flux of 0.8 to 2.1×10^{10} and the defining collimator ($z=86.5$ m) will see 0.3 - 0.7×10^9 . This is for an incident proton intensity of 5×10^{12} .

The collimators used in MC were formed of a pair of variable jaw collimators, one horizontally-defining and the other vertical. The total length of both was 10 to 12 ft. Each jaw was a rectangular piece of iron approximately 4"x8" transversely. Fig. 5.8.3 shows a CASIM calculation⁴⁷ for 30 GeV and 300 GeV protons on iron cylinders of different sizes. We have compared the CASIM shower containment predictions with GEANT. The GEANT predictions for a 1 m long iron cylinder is in good agreement with CASIM. For a length of 3 m the plateau of the GEANT curve is about 15% lower than the CASIM results while the shapes are similar. GEANT was also used to calculate similar shower containment curves for incident neutrons and K_L which gave essentially identical results as protons in GEANT. Based on these predictions, we have chosen 2m for the length of the primary collimator and a more conservative 3 m length for the defining collimator because of its proximity to the detector.

⁴⁷ CASIM , A. Van Ginneken & M. Awschalom, High Energy Particle Interactions in Large Targets, (1975);

A Van Ginneken, Fermilab Report FN-272 (1975).

Fig. 5.8.3 Fraction of incident energy deposited vs. radius for 30 GeV/c and 300 GeV/c. (From Van Ginneken and Awaschalom)

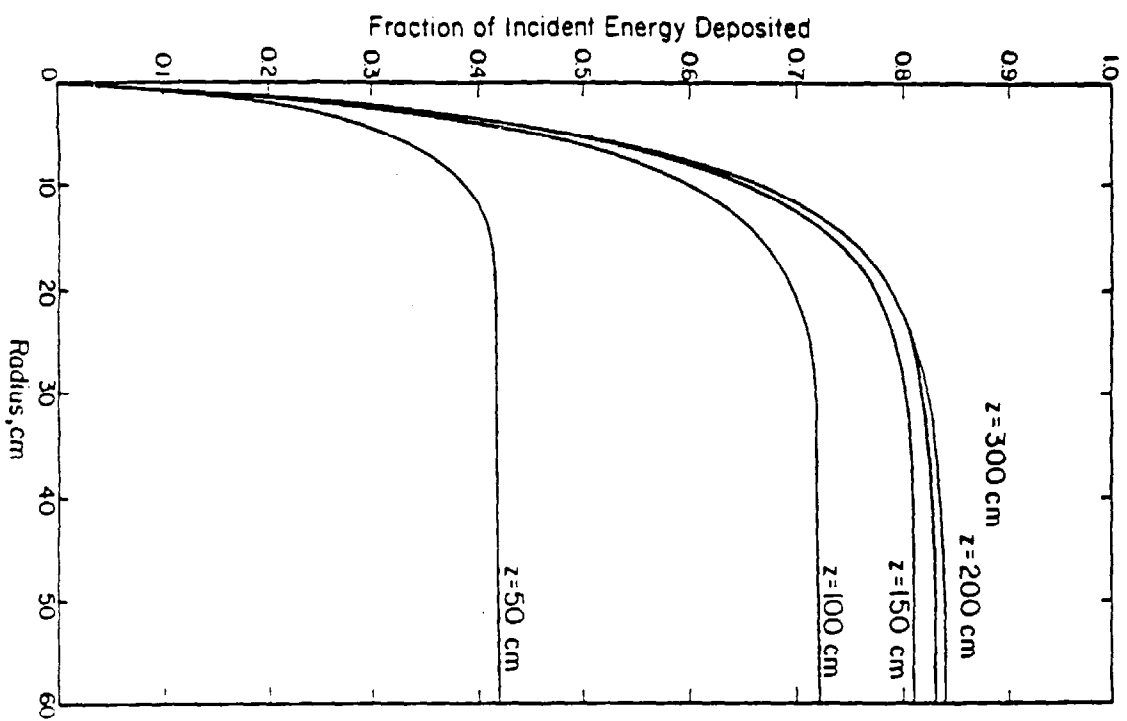


Fig. VIII.74. 30 GeV/c protons incident on a solid iron cylinder. Fraction of the incident kinetic energy deposited as ionization, plotted as a function of radius for various cylinder lengths. The beam of 0.3 cm x 0.3 cm cross section is centered on the cylinder axis.

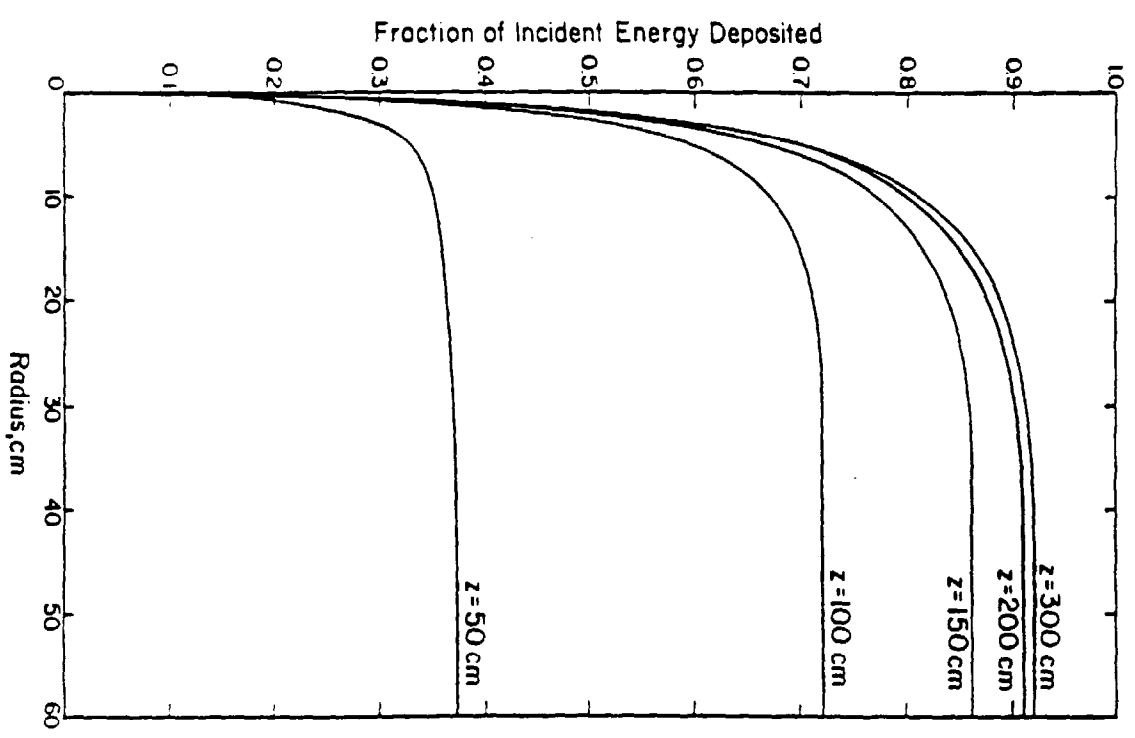


Fig. VIII.76. 300 GeV/c protons incident on a solid iron cylinder. Fraction of the incident kinetic energy deposited as ionization, plotted as a function of radius for various cylinder lengths. The beam of 0.3 cm x 0.3 cm cross section is centered on the cylinder axis.

5.8.4 Primary/Upstream Fixed Two-Hole Collimator

There is an existing collimator which may match our needs. Figure 5.8.4 shows one of these collimators. The design has a movable inner block with apertures to collimate the beam and a fixed outer iron shell. A great deal of experience with this design exists. The motion control is very accurate and reproducible. The radial shielding is currently about 10.5" to which we would add iron to bring the radial shielding to our 12" requirement. The effective shielding length (length of the inner block and downstream portion of the outer shell) is 1.9 m as is. The inner block will have two sets of holes; one for the standard beams and one for the optional larger solid angle beams (displaced from each other vertically in the inner movable block 4"x6").

Unfortunately, this existing collimator steel is slightly radioactive preventing machining which is needed to add the tungsten alignment masks (see section 5.9). Since this collimator is a "clean-up" collimator and not the defining collimator, we will eliminate the alignment masks on this collimator to minimize the modifications needed.

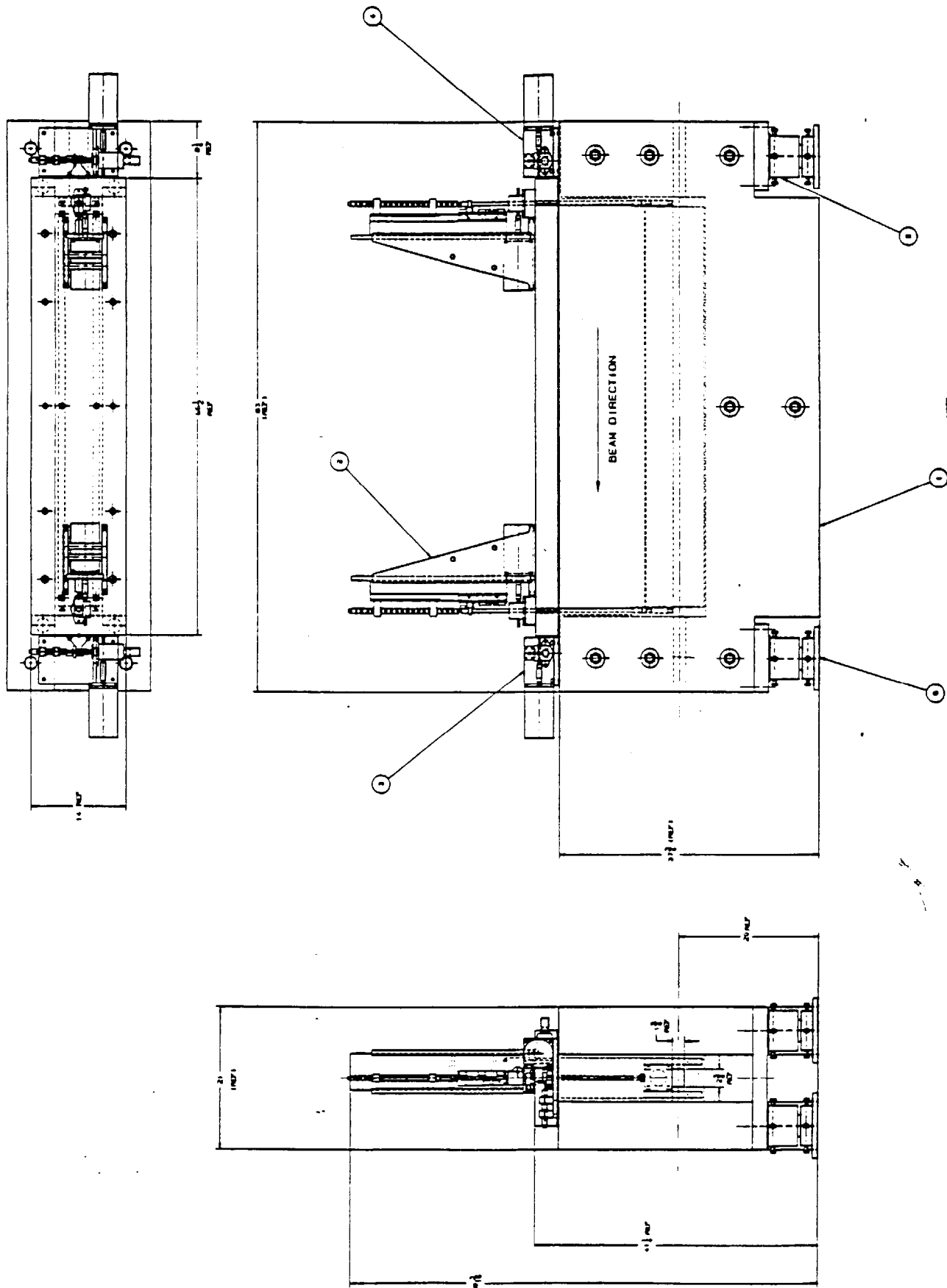


Fig. 5.8.4 Existing Collimator to be Modified for Primary Collimator

NOTE: 1. ADD WEIGHT OF SET POINTS AND BEAM LINE
2. ADD WEIGHT OF COLLIMATOR DRIVE MOTOR ATTACHMENT.

APPROX. WT. = 10,000 LBS.

QTY	ALIAS	DESCRIPTION OR DIM.	UNIT
1	ME-272811	140R12 DRIVE ASSEMBLY (D.L.)	
1	ME-272258	140R12 DRIVE ASSEMBLY (D.L.)	
2	ME-272798	140R12 DRIVE ASSEMBLY	
1	ME-272103	PINOLE COLL. BODY (S.S.)	
1		DESCRIPTION OR DIM.	

PARTS LIST	
QTY	DESCRIPTION
1	ME-272811
1	ME-272258
2	ME-272798
1	ME-272103
1	PINOLE COLL. BODY (S.S.)

PERM NATIONAL ACCELERATOR LABORATORY	
UNITED STATES DEPARTMENT OF ENERGY	
PINOLE COLL. COMPLETE AS	
NE-4	
RD/MD	

5.8.5 Defining/Downstream Fixed Two-hole Collimator

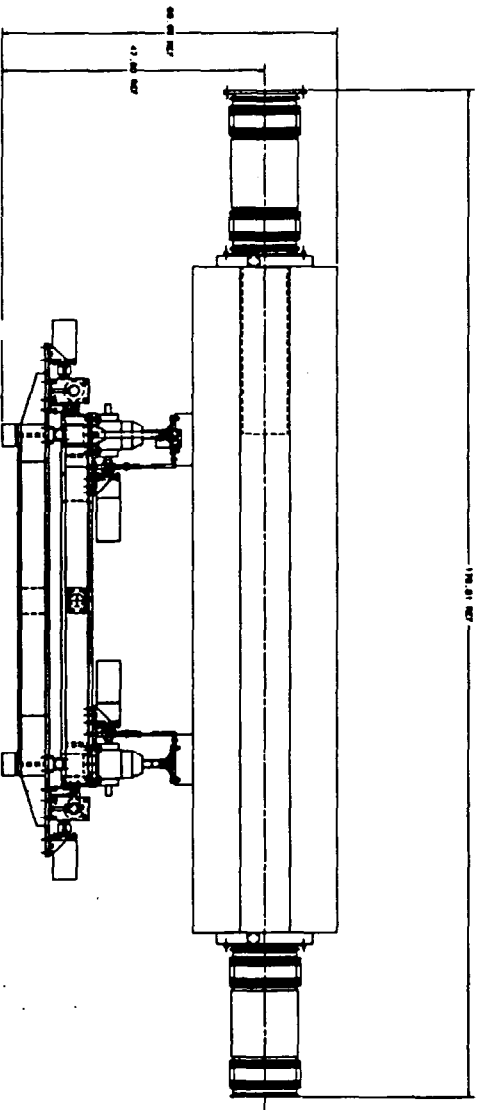
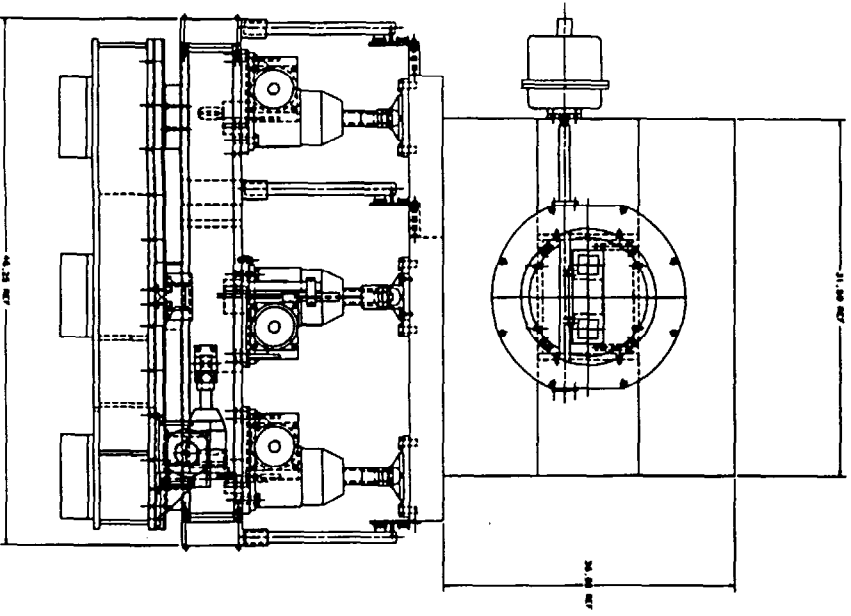
The defining collimator differs from the primary collimator in that it is located close to the detector and is also required to be a vacuum device. Because of this vacuum requirement existing collimators such as being used for the primary are unsuitable. The general design features as discussed earlier are a fixed hole collimator with a neutral channel insert which can be manually changed to another hole size if needed. Such a change of inserts is expected to take approximately 8 hours.

Making a collimator insert with a 1" tungsten liner around the neutral channel reduces the spray off the collimator by about 50% according to GEANT. The majority of this spray off the defining collimator is low energy photons. These studies also indicate that using the jaw collimator to reduce the flux on the defining collimator reduces the collimator spray as effectively as the W liner assuming 5-10 mils alignment and motion control accuracy on the jaw collimators. Given the cost tungsten we have chosen iron inserts rather than tungsten and will rely on the jaws to reduce backgrounds from the defining collimators if necessary.

We have chosen 3 m for the length of the defining collimator because of its proximity to the detector. Again we have used CASIM calculations (fig. 5.8.3) as well as our own GEANT studies to select this length.

Following this defining collimator is a magnetic sweeper which also provides additional hadronic shielding. We could, if necessary, also place approximately 1 m more of shielding between the defining collimator and the sweeper. The location of this collimator is the same as our most downstream collimator in MC. Previous studies of the effect of varying the MC sweeper just downstream of this collimator indicated very small charged particle contributions to the trigger (<5-10%). In fact we may choose in KTeV to run with this sweeper off as in the past. However the sweeper may be helpful in slightly reducing collimator spray; but it reduces the acceptance for lambda triggers in E799II by a factor of two. Fig. 5.8.5 shows the engineering design for

Fig. 5.8.5
Defining Collimator



the defining collimator. It includes remote adjustment transverse to the beam on each end as well as small rotation about the beam axis.

5.8.6 Alignment and Mechanical Tolerances

The criteria for setting the defining collimator tolerances are:

- a) The beam size and position at the CsI affected by no more than 0.5 mm from the sizes and alignment of the various collimator apertures.
- b) The areas of the two beams must be equal to within 1%.

These criteria impose a horizontal and vertical tolerance of ± 200 microns.

The criteria for setting the primary collimator tolerances come from :

The size of the beam at the CsI, including scattered rays must be less than 13 cm to provide a minimum of 1 cm clearance between the beam and the CsI edges (see Fig. 5.8.6). In order not to have the primary collimator define the beam, we have a clearance of ± 500 (1000) microns in the horizontal (vertical). The mechanical and positioning error is approximately ± 150 microns. Therefore, an alignment tolerance of ± 200 microns is sufficient allowing some margin for positional instability. The alignment of the slab collimator is less critical; using the same criteria as for the primary collimator, a tolerance of ± 1.3 mm is obtained.

5.9 Beam Instrumentation/Monitoring

Monitoring the alignment of the neutral beam elements to the required tolerances is critical to the KTeV program. The alignment section of this report discusses the procedures planned by the FNAL alignment department. We also plan to monitor the alignment using the beam itself. A

system to do this is outlined in the Design Report.⁴⁸ The defining collimator has tungsten masks (0.50" of tungsten) on both the upstream and downstream ends which flip in and out of the beam with a pattern of holes or slits which can be detected by a beam alignment monitor just downstream of the CsI beam holes. This scheme requires the insertion of masks, removal of the filters, and possibly a reduction in primary beam intensity to make a photon beam. Even a crudely segmented detector can be used to monitor

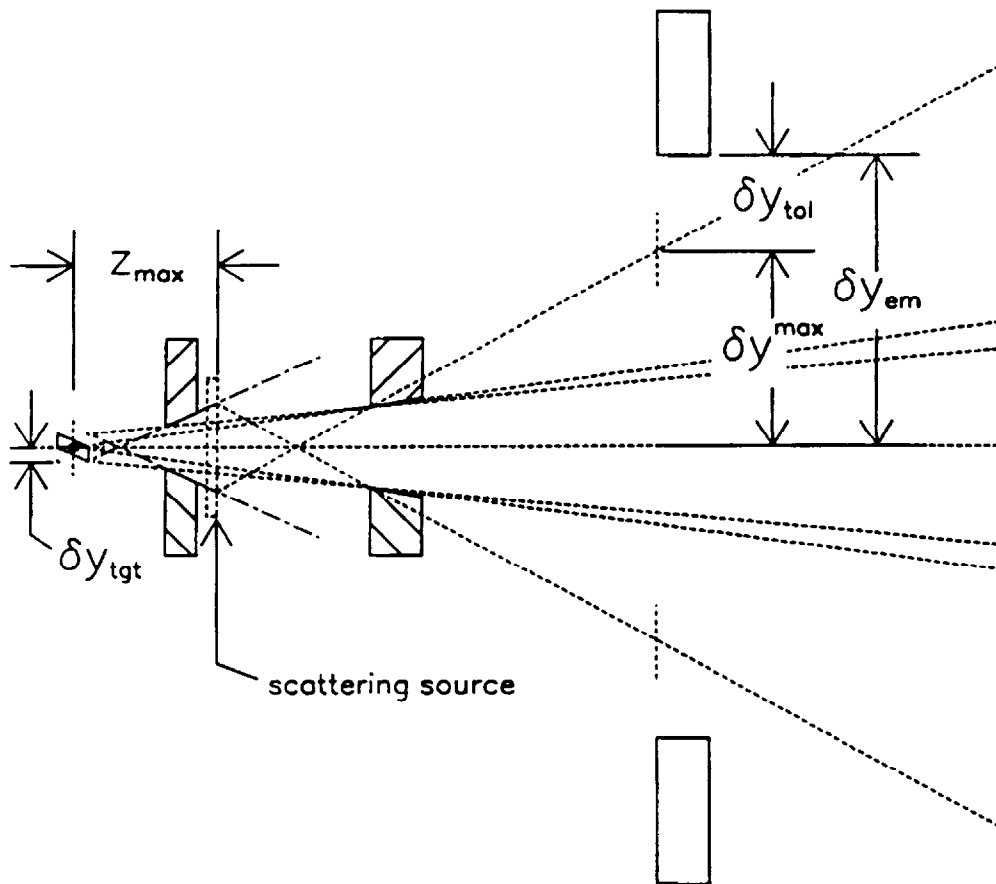


Figure 5.8.6 Elevation view of the collimator system showing the downstream most filter location and illustrating the clearance between the calorimeter and the scattered rays.

the alignment quite accurately (± 50 microns). For example, Fig. 5.9.1 shows a mask pattern which could be detected by 5 scintillator counters. In addition we would require a single veto trigger plane scintillator upstream of a tungsten convertor (0.10") followed by additional planes (2 or 3) of scintillator

⁴⁸ KTeV Design Report, January 22, 1992 and private communication , M. Crisler.

which could be used to select events with pulse height consistent with an e^+e^- pair. This profile detector will be followed by the back-anti which could provide a threshold cut on the converted pair. The mask patterns, backgrounds, scattering as well as the required detector are being optimized using GEANT. Preliminary results indicate background levels are small (Fig. 5.9.2). Backgrounds from hadrons are approximately 10^{-3} of the hadron flux. We are also planning to build a profile monitor which could have sufficient segmentation to take a snapshot without the above requirements. To obtain the segmentation we will build a horizontal and a

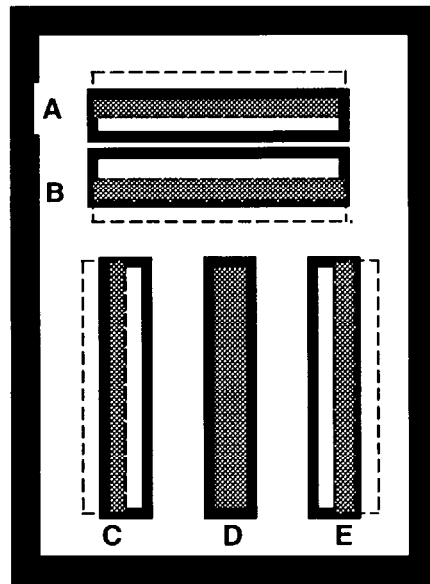


Fig.5.9.1 Signal pattern from perfectly aligned pair of masks (shown in shaded area). Dotted line represents one mask while heavy line represents the other mask. The detected signal D represents perfectly aligned holes in both masks while the others represent holes of the same area aligned perfectly but offset by $0.5 \times$ area. For example, a vertical translation down of the dotted mask would produce a larger signal A compared to B indicating the misalignment.

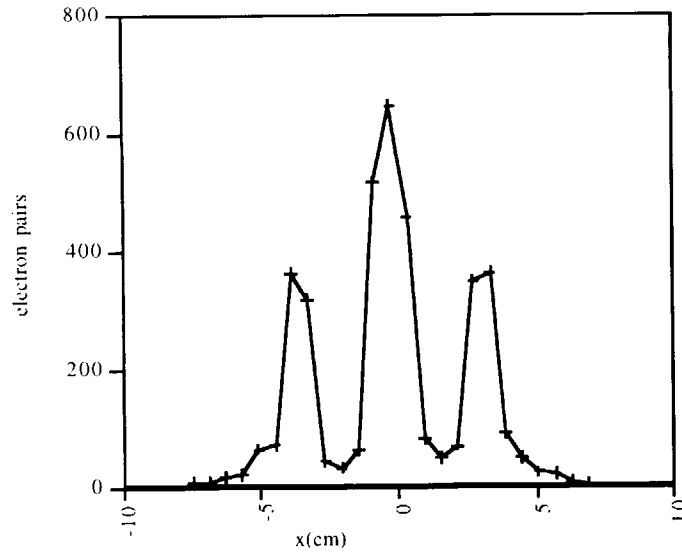


Fig.5.9.2 Pattern of detected electron pairs in alignment/profile monitor from 20,000 incident photons simulated using GEANT. Selection criteria is two charged tracks originating in converter with total electromagnetic energy > 2.5 GeV.

pair of vertical scanning scintillators (2 mm wide) to sweep across both beam holes which will be placed downstream of the tungsten converter. Both the alignment monitor and the profile monitor should be placed in a single unit which can be accurately placed and have an out position for normal data taking.

5.10 The Lambda Polarized Beam and Spin Rotations vs Sweepers

One of the considerations that enters especially into the magnets needed in the neutral beam is that of lambda production and polarization. In the following discussion, we ignore the finite targeting angle in the horizontal and assume that there is targeting at 4.8 mrad in the vertical direction. The polarization is rotated if the lambda travels through a field perpendicular to the polarization direction of the lambda. The polarization is unaffected by a field along the direction of the polarization. In the KTeV configuration, the production is vertical, so the polarization will be along the x axis of the spectrometer.

The first 3 magnets in the beamline have vertical fields and thus cause a rotation of the polarization. The angle is 11.2 degrees/(Telsa-meter). The

rotation by the target sweeping magnet, E8/Hyperon, and Mu-Sweep II is 21, 142, and 117 degrees respectively, for a total of 280 degrees. The plan is to reduce this by lowering the current slightly in the sweepers to give 270 degrees so that the initial polarization along the x axis is rotated to lie along the z axis. Then the next magnet in the beamline (spin rotator magnet-modified 20' long B2 with 4" x 4" aperture) will rotate the polarization into the $\pm y$ axis depending on the spin rotator magnet polarity. The field required is 8.04 Telsa-m while the spin rotator can provide up to about 9.0 Telsa-m.

5.11 Secondary Beam Simulations of Radiation Damage/Backgrounds

Two beams were simulated. In normalizing to particle fluxes through the calorimeter beam holes, for E731/E832 the regenerator beam was ignored compared with the more intense vacuum beam. For E799I/II intensity is taken to mean two beams. A week is taken to be 1×10^4 pulses. GEANT version 3.16 with the FLUKA hadronic shower generator comprised the software platform. The simulations of E799I/II were rerun with the GHEISHA generator to compare predictions. Differences in calorimeter radiation damage between the two generators are about 10%.

5.11.1 Comparison of Data and Simulations with E731 and E799-I

E731

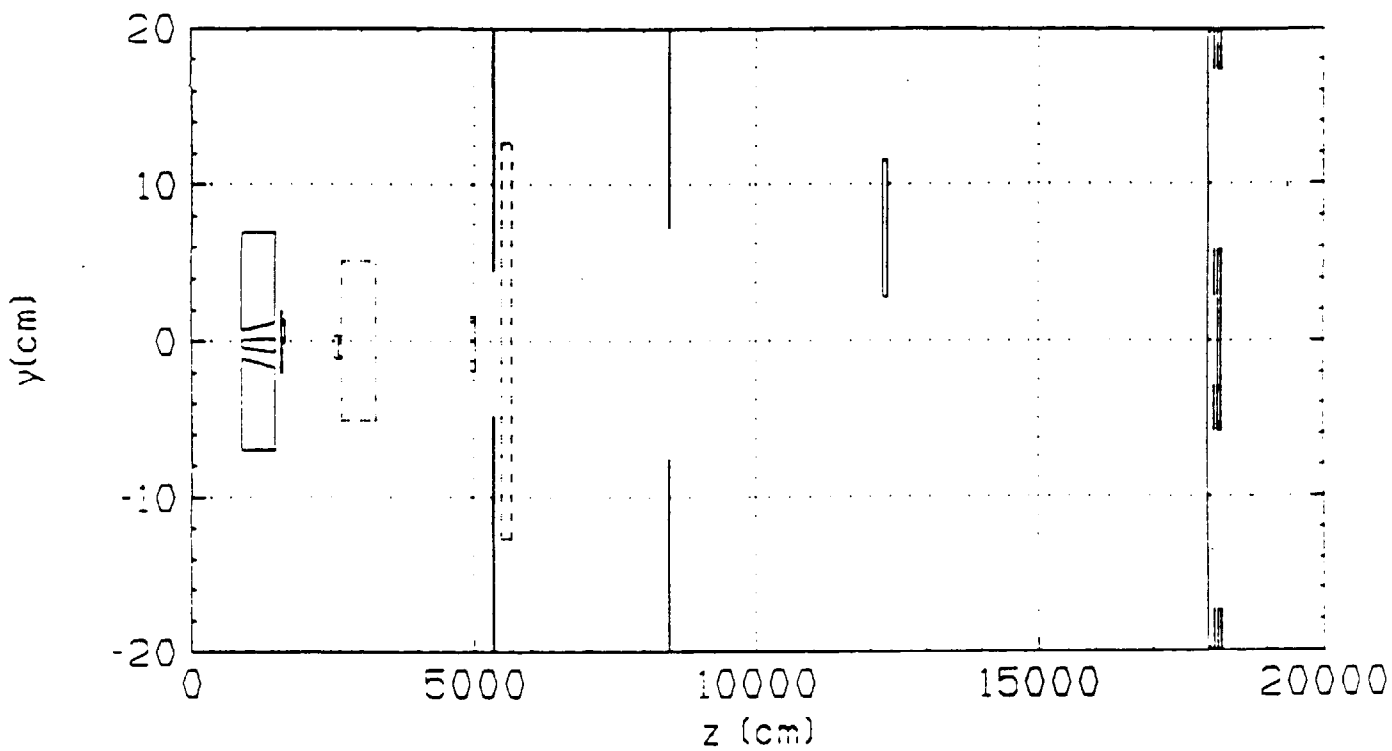
The E731 collimator positions are shown in Fig. 5.11.1. Even on this crude scale some misalignments can be seen: most fundamental is that the two-hole collimator did not precisely aim at the calorimeter beam holes. It is apparent after tracing a few rays that the upper collimator hole passes slightly more of the entering beam (the simulation gives about 10%). Fig. 5.11.2 shows the actual data for the E731 beams ⁴⁹.

⁴⁹ J.R. Patterson , Determination of $\text{Re}(\epsilon'/\epsilon)$ by the Simultaneous Detection of the Four $K_{L,S} \rightarrow \pi\pi$ Decay Modes, Dec.1990, U. Chicago dissertation.

Beam elements in the simulation (see Figure 5.11.1) were:

- 1.) Two-hole collimator
- 2.) 50 cm Be filter
- 3.) 7.5 cm Pb filter
- 4.) 45 cm Be shadow absorber in the regenerator beam
- 5.) Fe slab at 23 meters
- 6.) Sweeping magnet at 30 meters
- 7.) Fe slab at 50 meters
- 8.) Vertical aperture jaws at 51 meters
- 9.) Horizontal aperture jaws at 53 meters
- 10.) Sweeping magnet at 57 meters
- 11.) Vertical aperture jaws at 83 meters
- 12.) Horizontal aperture jaws at 84 meters
- 13.) Sweeper magnet yoke at 119 m (no field)
- 14.) Regenerator
- 15.) Trigger counters (TC)
- 16.) Collar anti (CA)
- 17.) lead glass and beamholes

(a) Elevation View.



(b) Plan View

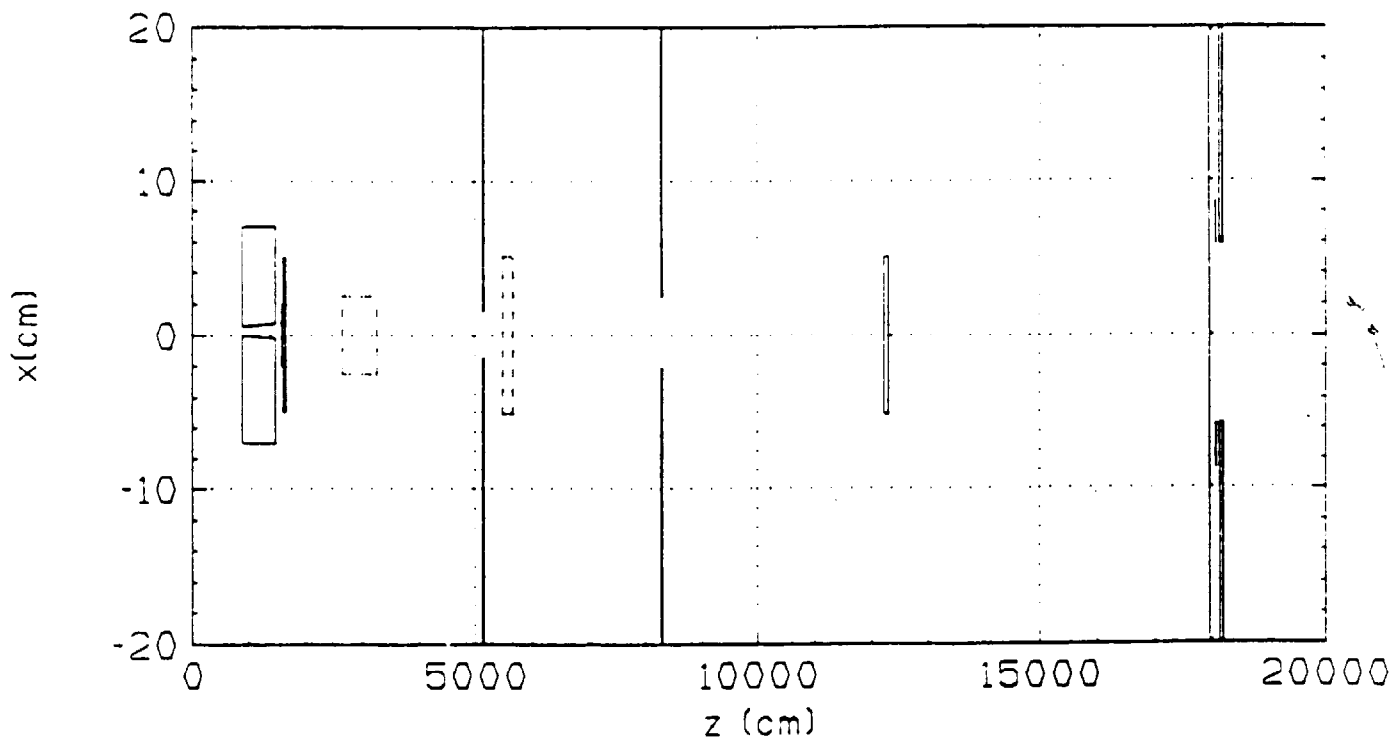


Fig. 5.11.1 Collimators, Be/Pb filters, B,C banks, Regenerator

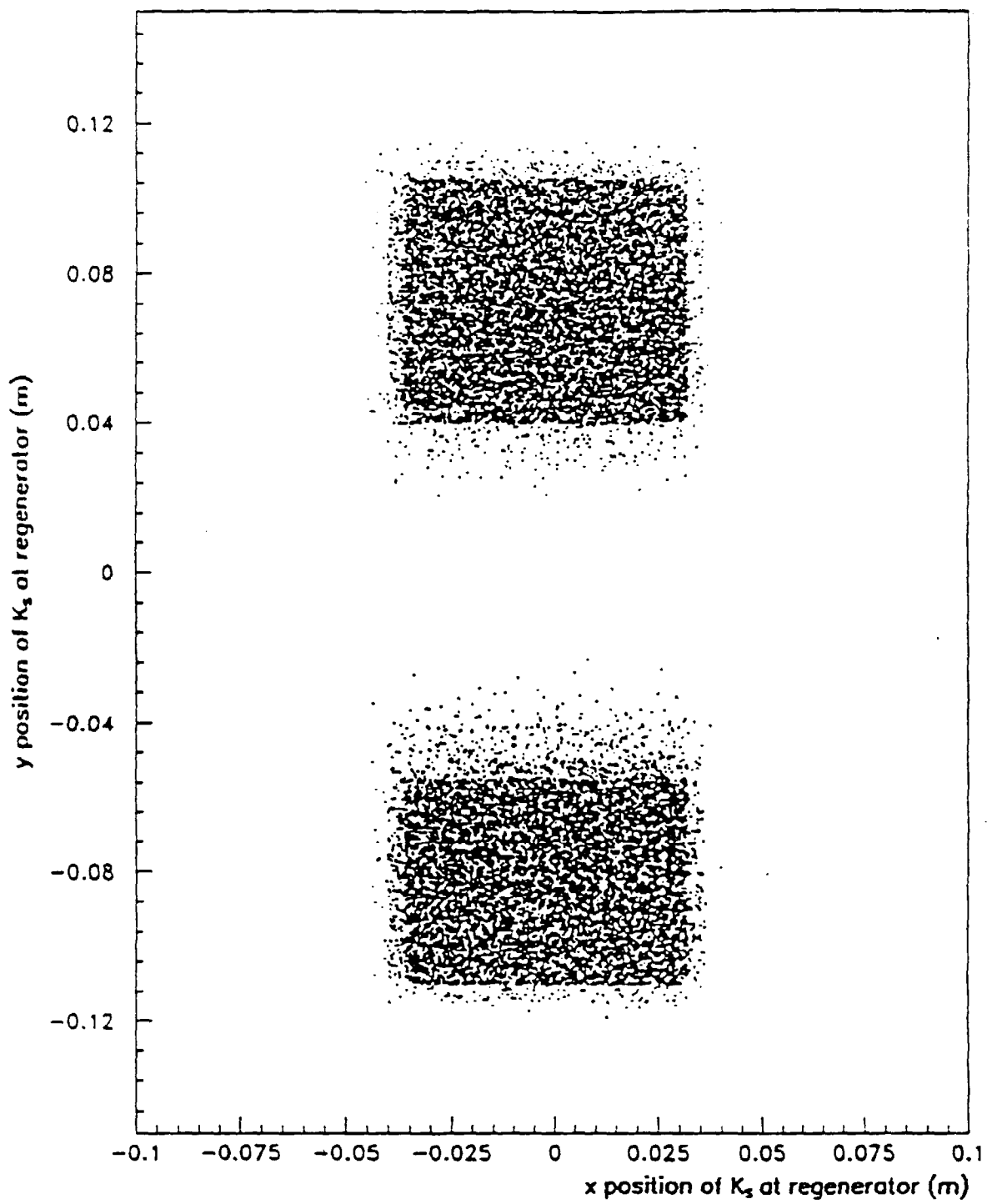


Fig. 5.11.2 The transverse position of the reconstructed kaon at the plane of the regenerator.

Material of all the elements was simulated in GEANT, except for some of the sweeping magnets iron (items 6 and 10) which were simulated by discarding any charged tracks that passed through them. In addition, particles that originated upstream of the last jaw pair (item 12) were not followed unless their energy exceeded 1 GeV. Downstream of 84 meters all tracks with $E > 20$ MeV were followed. The simulations also included a vacuum window, helium, and the drift chamber materials. Runs were made with this material replaced by vacuum and also air. In addition, runs were made with and without the TC.

The upstream aperture of the two-hole collimator was randomly filled with track-starting points and the target was randomly filled with the corresponding particle origins. The direction so defined was assigned to a momentum selected from the Malensek distributions. Encounters with the walls of the two-hole collimator were simulated, and a few cases were found in which hadronic elastic scatters in the collimator eventually led to calorimeter activity. After having done several simulations where it was apparent that inelastic scatters in the Be, Pb, and two-hole collimator consumed a large fraction of CPU time but did not lead to activity in the lead glass, events were dropped in the remaining simulations if the beam particle interacted inelastically in any of these elements.

Figure 5.11.3 shows some results of a neutron and a K_L run with all parameters nominal, set to what was measured for the experiment. The run statistics generally give 10^4 or more beam particles through the lead glass holes. Figure 5.11.3 shows an attrition of 30-50 between starting particles (Figure 5.11.3a, c) and those that get past the calorimeter (Figure 5.11.3b, d); momentum of the survivors is not much different from the starters except for the decay loss of low energy K_L due to their small Lorentz factor. Figures 5.11.3 e and f show energy absorbed in the lead glass as a function of x, y position of the individual ionization deposits. The cell contents are weighted by the absorbed energy and therefore give the simulated radiation damage. Figures 5.11.3 g and h show the central region enlarged. Damage due to neutrons is more centered than for the K_L 's.

EXP731. TRIG, CA. Pb, Be Filters

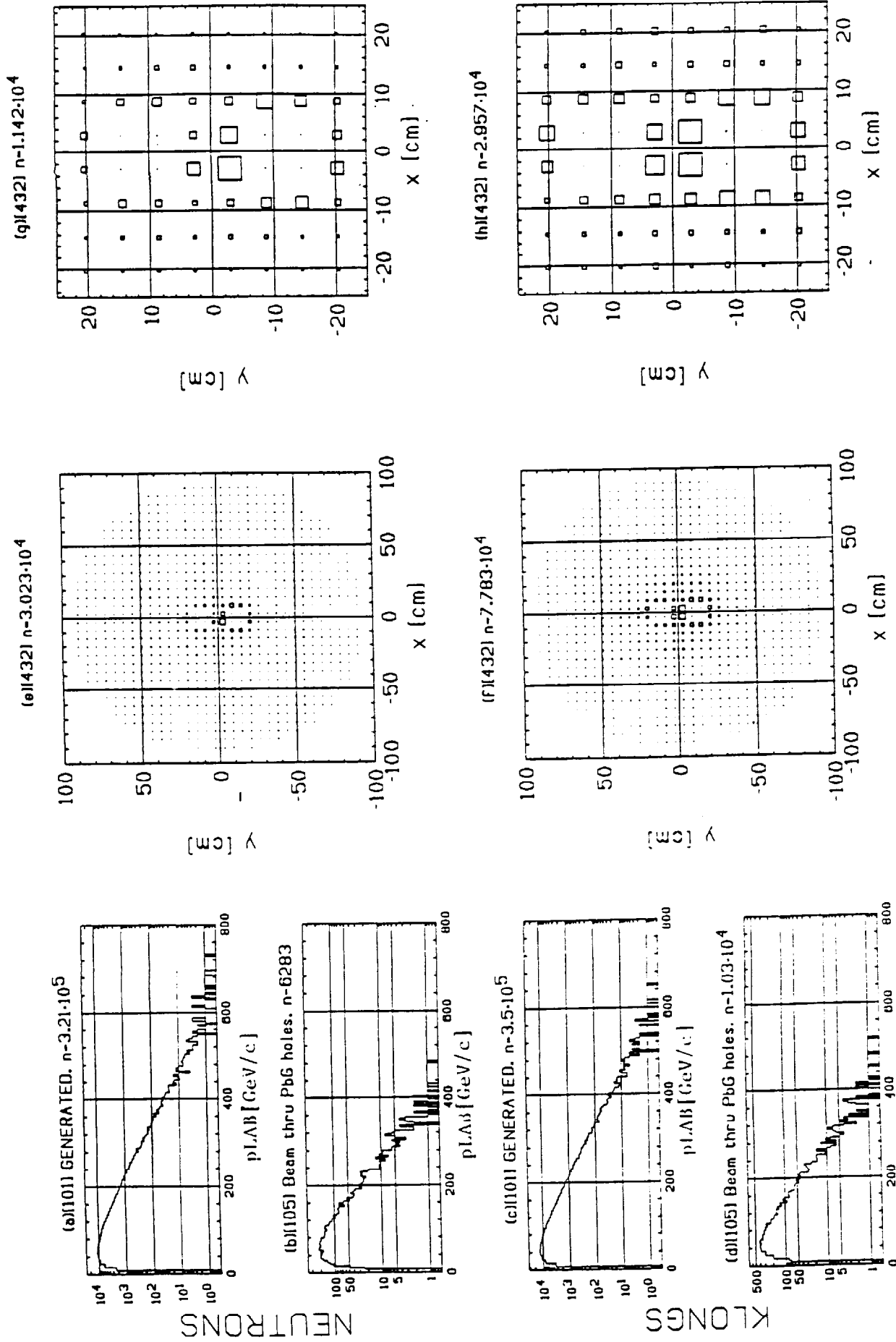


Fig. 5.11.3 Energy deposited in Leadglass.

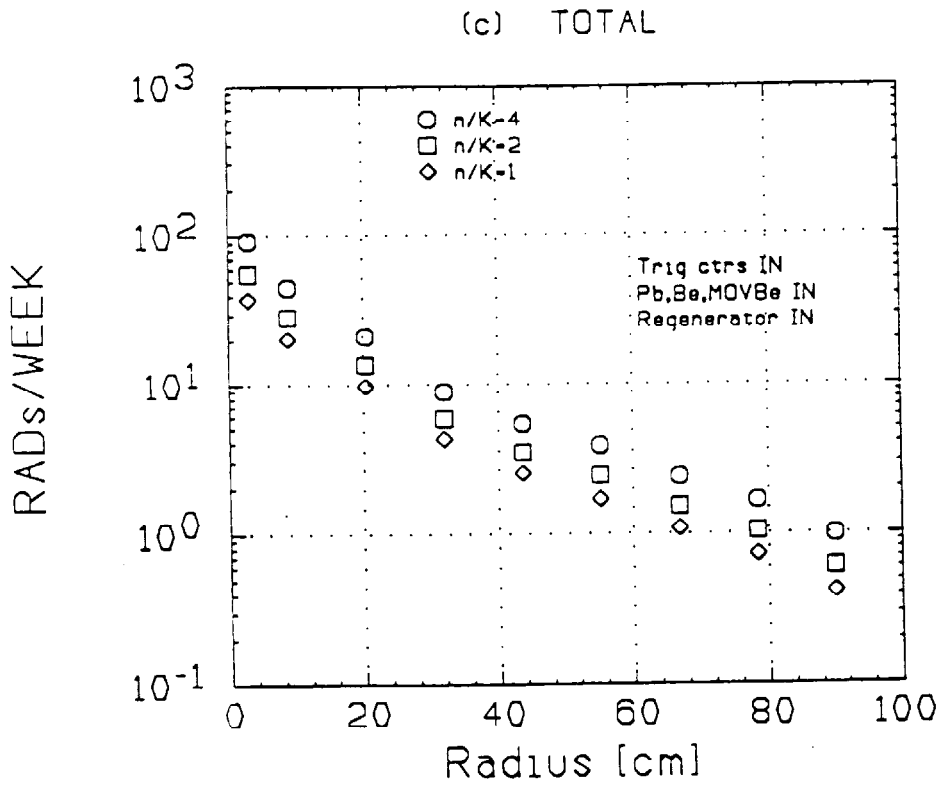
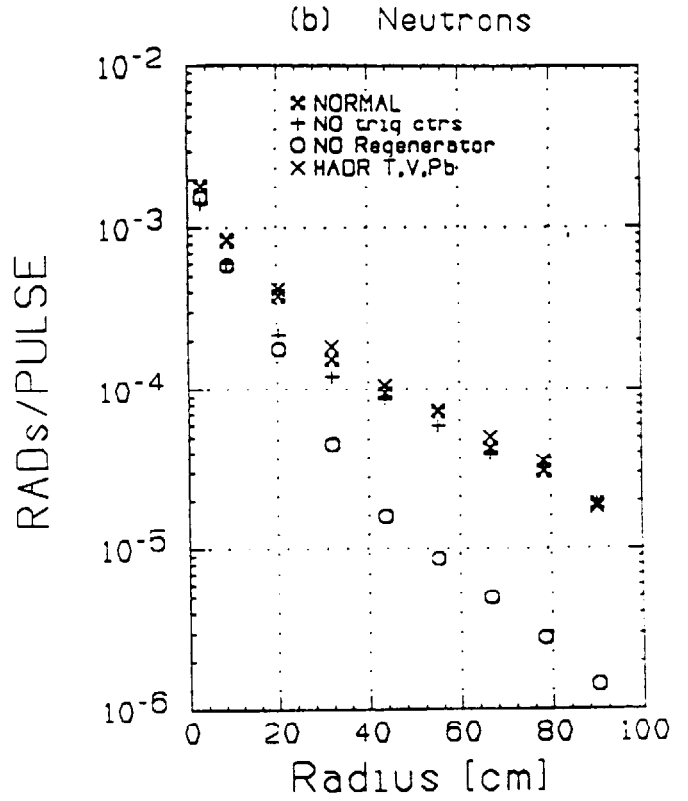
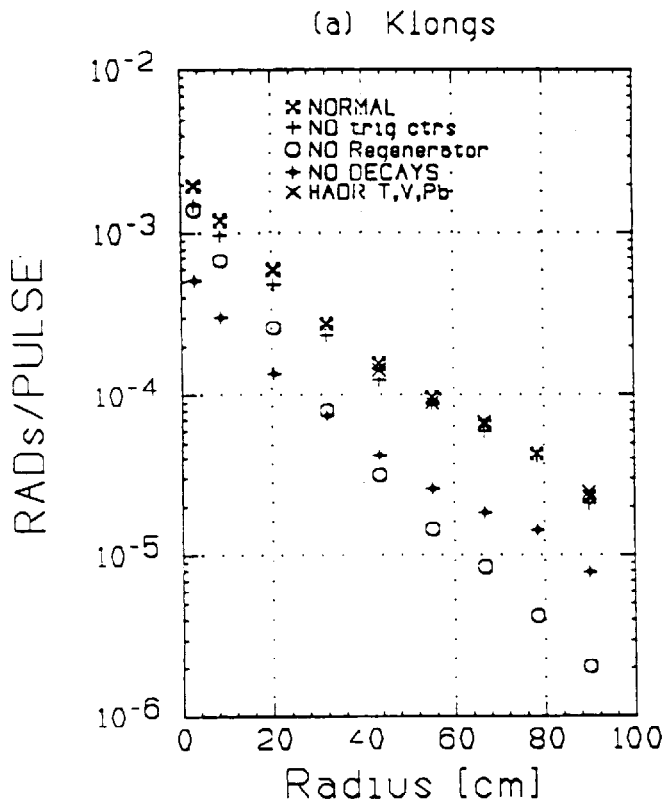


Fig. 5.11.4 EXP731. Radiation vs radius

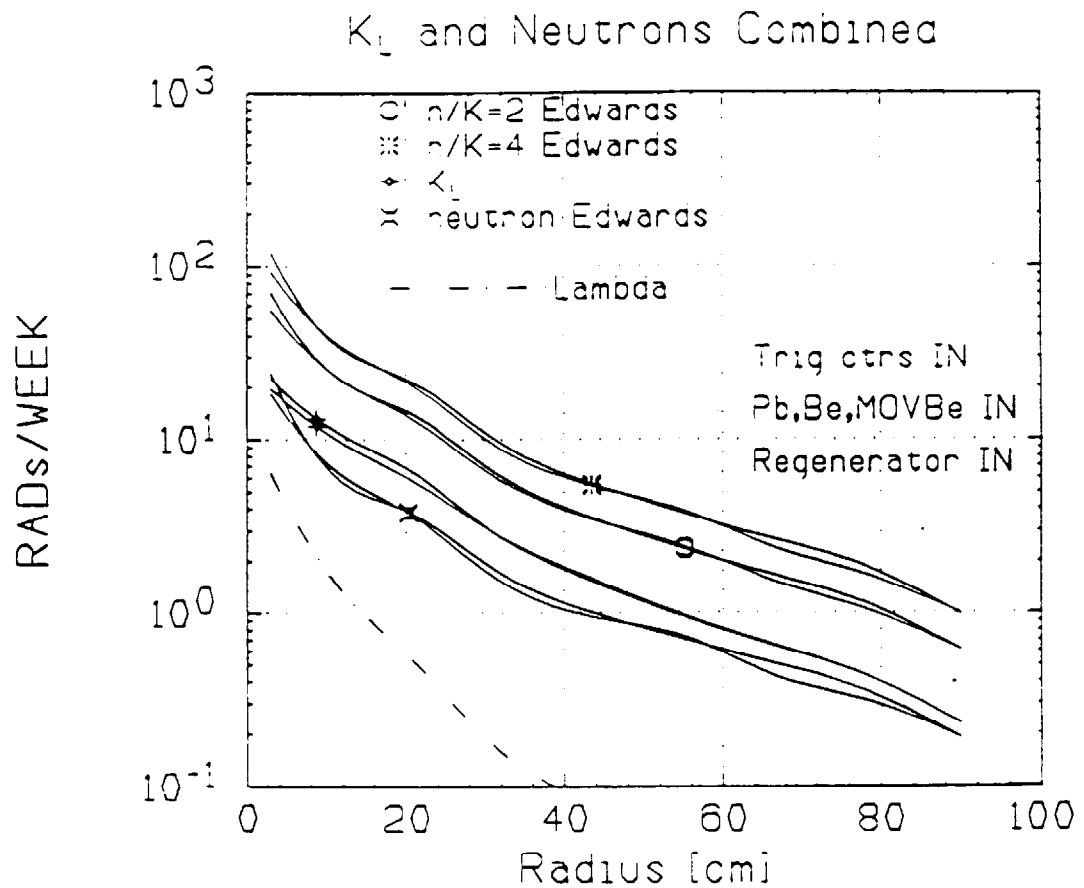


Fig. 5.11.5 Radiation vs radius. EXP731.

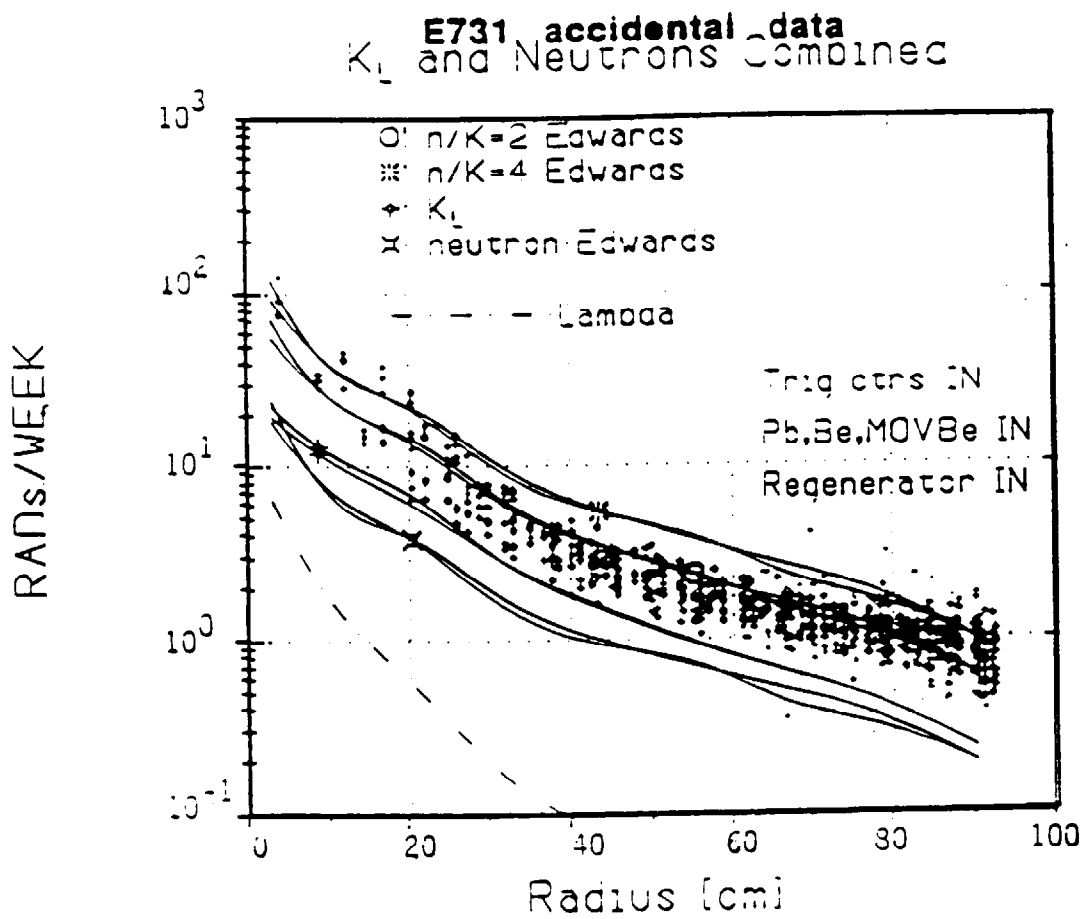


Fig. 5.11.6 Radiation vs radius. EXP731.

E799-I

Collimator positions are much closer to perfect alignment than for E731. The simulation runs were done essentially the same as for E731 except (1) regenerator and shadow absorber were absent, (2) there was no Be filter, and (3) TRD material, $2\%X_0$ of polypropylene, was added. The other TRD components were ignored. The kaon flux increased from 10^7 to 8.5×10^7 . Figure 5.11.7 show energy absorbed in the lead glass due to K_L , n. The simulation was repeated without the TC's and TRD's; these detectors contribute about 1/3 of the K_L -induced background and $\approx 3/4$ of the neutron-induced background. Figures 5.11.8-9 show the results again with several assumptions on the neutron flux. This comparison matches best if $n/K_L=4$ for E799 or $n/K_L=2.8$ (E731 vacuum beam).

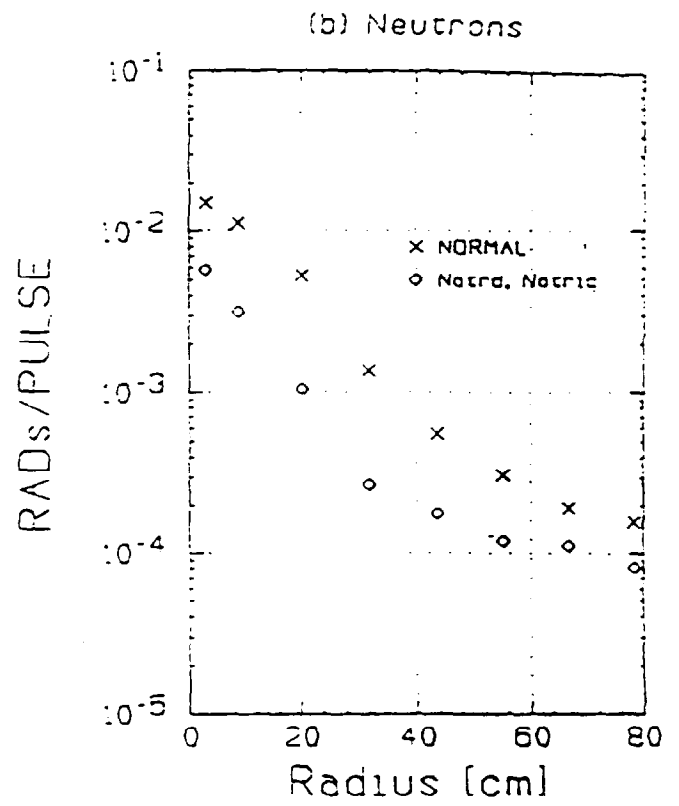
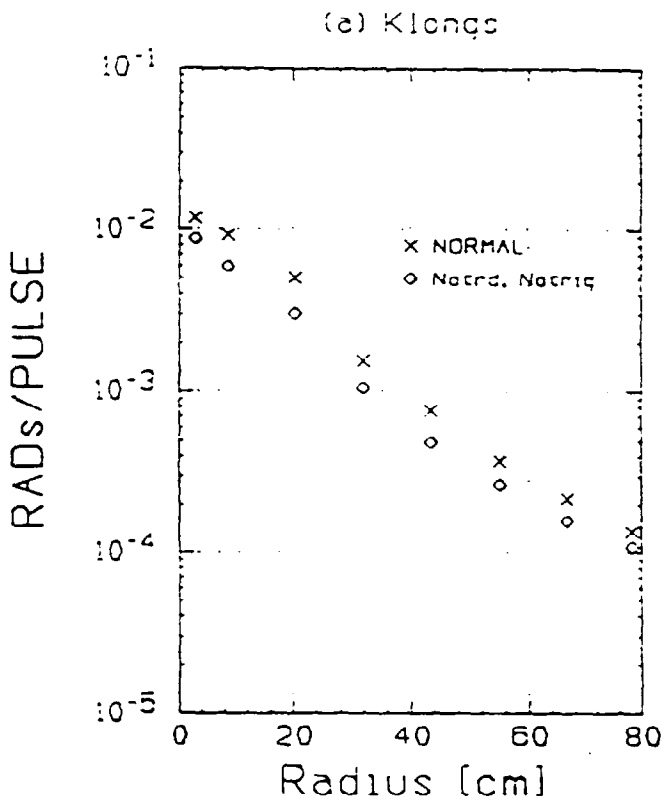


Fig. 5.11.7 EXP799-I. Radiation vs radius.

K_L and Neutrons Combined

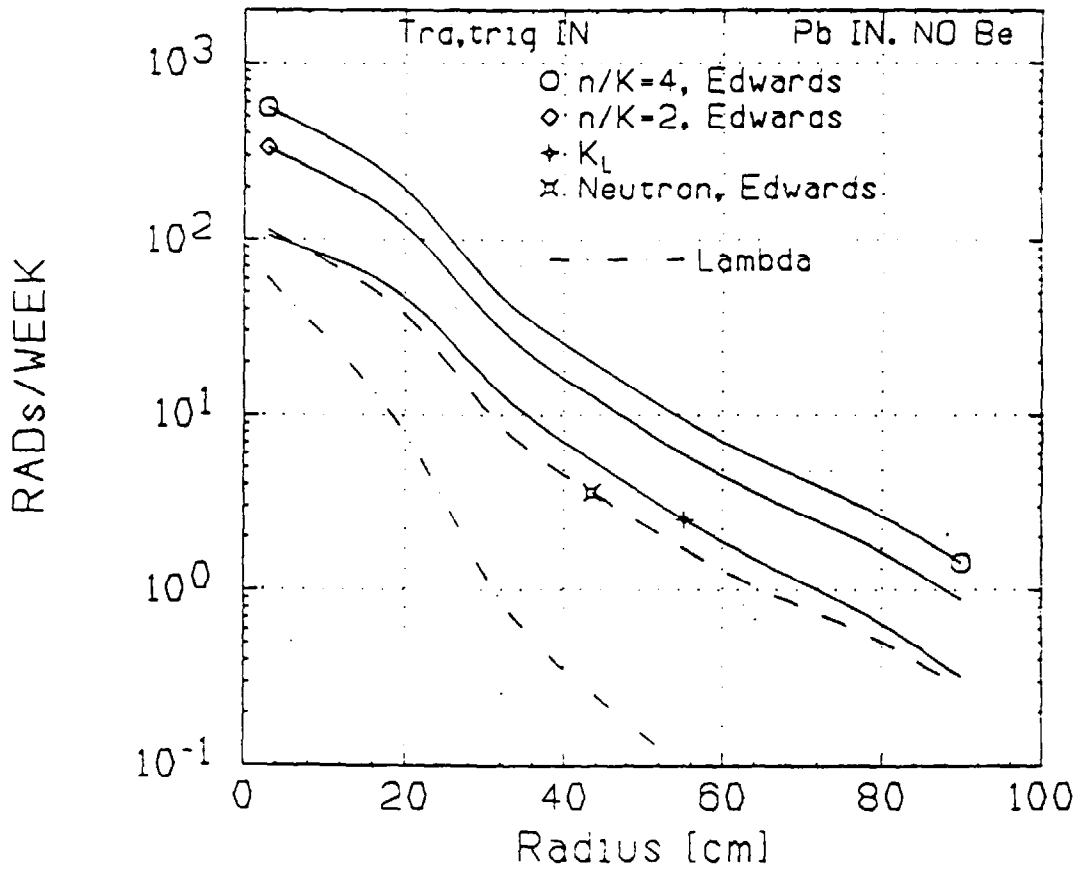


Fig. 5.11.8 Radiation vs radius. EXP 799-I.

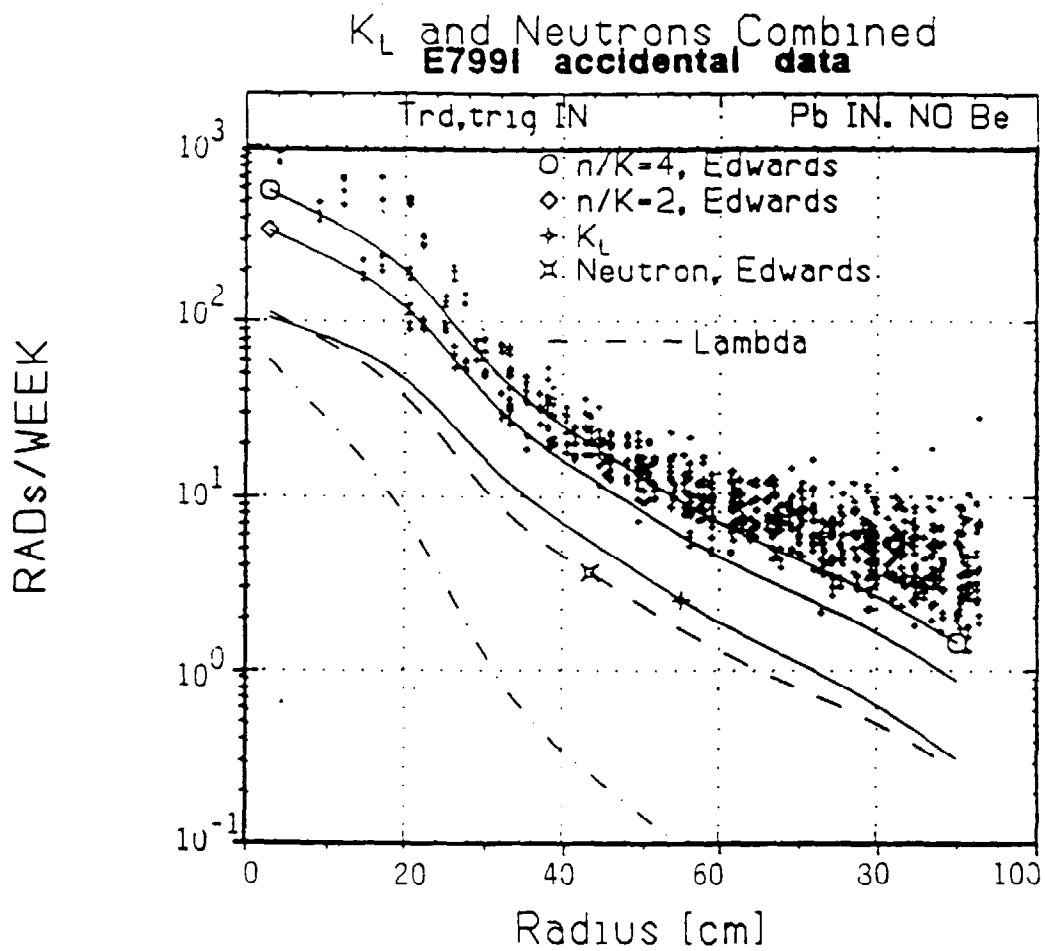


Fig. 5.11.9 Radiation vs radius. EXP799-I.

Figure 5.11.10 shows the origin of particles that enter the lead glass for the K_L runs. It is organized into four quarters, split vertically by weighting: (top six plots) equal weights for all hits, or (bottom six) hits weighted by energy of the particles that enter the lead glass. The horizontal split depends on whether the B and C banks and the TRD's are in or out. Figure 5.11.10a shows the vertex z for each particle that enters the upstream face of the lead glass. There are spikes near $z \approx 900$ centimeters where tracking starts at the entrance to the two-hole collimator, at $z \approx 1600$ (the Pb filter), in a region at $z \approx 5000$ where the last slab and upstream jaws are located, at $z \approx 8000$ at the downstream jaws, and near $z \approx 18000$ at the TRD and B, C counter banks. The final spike lies in the bin $18050 < z < 18100$ which contains the collar anti counter. Beneath each major plot, the upstream ($9 < z < 16$ meters) and downstream ($176 < z < 185$ meters) regions are expanded.

The number of hits that can be traced back to the two-hole collimator entrance and the Pb filter is relatively small (~ 900), due to TC ($\sim 40,000$) and due to TRD ($\sim 10,000$). On the other hand, the energy-weighted plots, Figures 5.11.10c (with B, C, TRD) and 5.11.10d (without B, C, TRD) show that these are on a par for radiation damage with the material right in front of the lead glass. The detailed z -cut plots allow the particular collimator or filter element to be isolated. The area under the broad- z distribution (decays) between the spikes is $\approx 40\%$ of the total area, comparable to that under the spikes.

Figure 5.11.11 shows the same set of plots for a neutron beam. The main difference is the near absence of decays. The GEANT prediction is about half of the pipe block energy or damage is correlated with interactions in

either the TRD or TC. A recent study of E799I accidental data⁵⁰ finds 44% of the pipe block energy is correlated with TRD and TC interactions in good agreement with the Monte Carlo. This same study also measured the rate on the hottest drift chamber wire in the most upstream chamber in E799I after subtracting out the muons from our upstream target and beam dump gives 26 kHz for the hottest wire. While our GEANT model of the secondary beam charged particle flux indicates about 17 kHz for E799I from K_L decays only.

⁵⁰ private communication, R. Tschirhart.

K_L BEAM

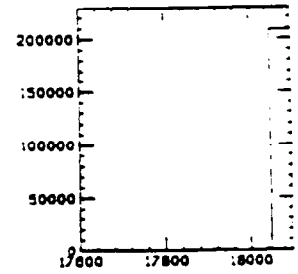
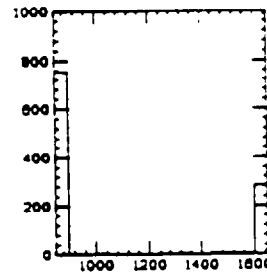
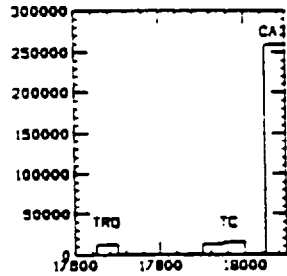
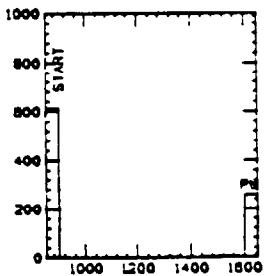
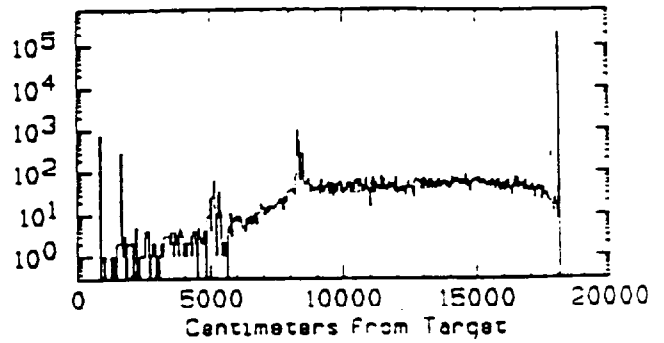
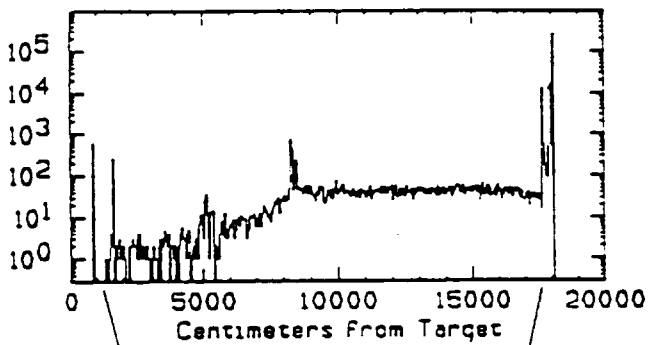
nthru=8.148·10⁴

EQUAL WEIGHTS

nthru=9.449·10⁴

(a) TRD,B,C

(b) NO TRD,B,C



WEIGHTED by ENERGY

(c) TRD,B,C $\Sigma=4.838 \cdot 10^5$

(d) NO TRD,B,C $\Sigma=3.945 \cdot 10^5$

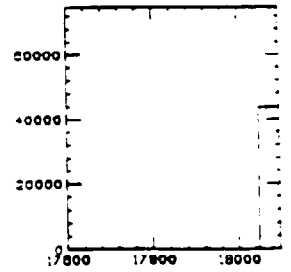
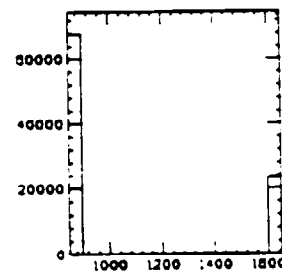
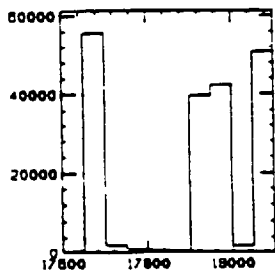
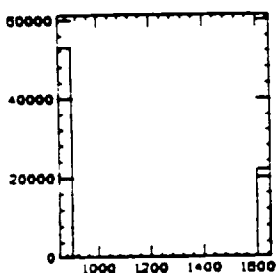
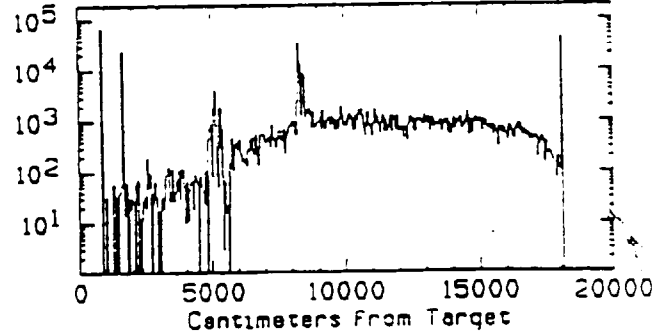
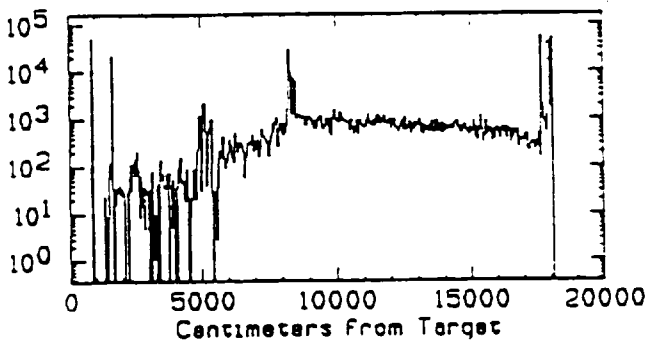


Fig. 5.11.10 Z-origin of particles entering PbG. E799-I

NEUTRON BEAM

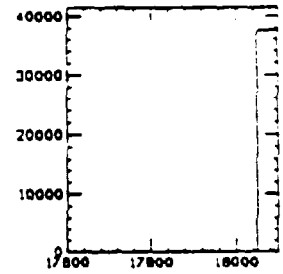
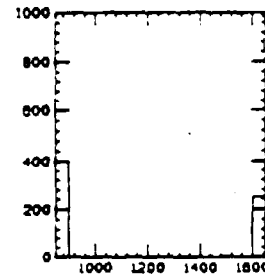
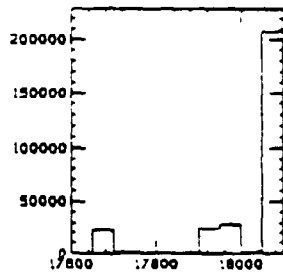
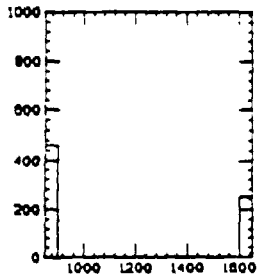
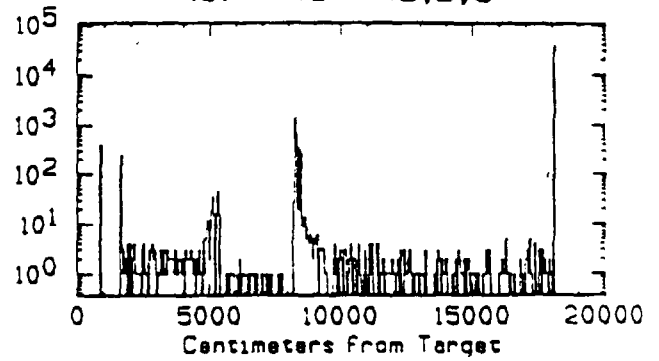
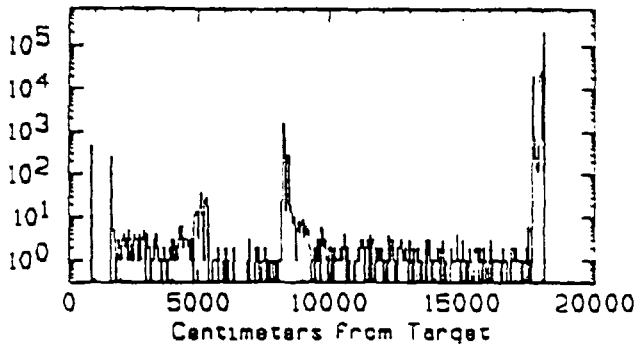
nthru=8.356·10⁴

EQUAL WEIGHTS

nthru=7.456·10⁴

(a) TRD,B,C

(b) NO TRD,B,C



WEIGHTED by ENERGY

(a') TRD,B,C $\Sigma=5.647 \cdot 10^5$

(b') NO TRD,B,C $\Sigma=2.227 \cdot 10^5$

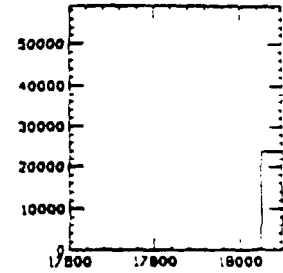
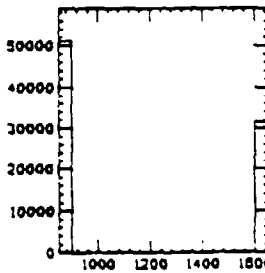
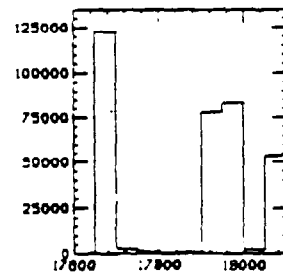
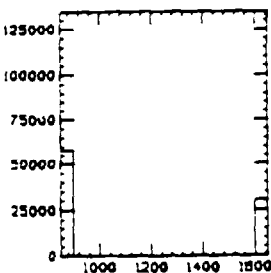
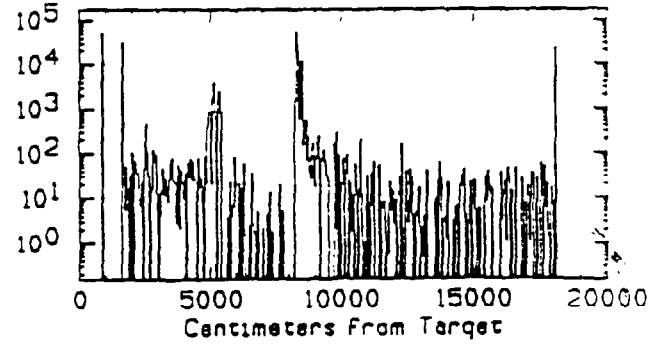
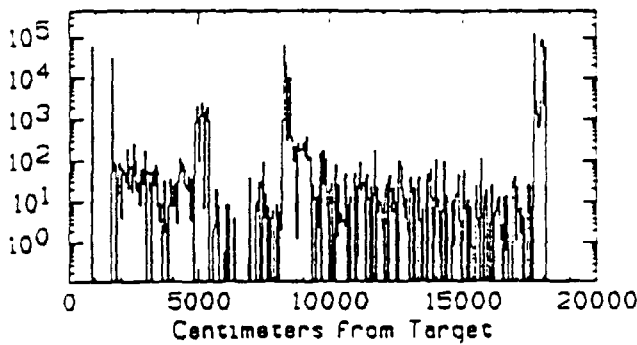


Fig. 5.11.11 Z-origin of particles entering PbG. E799-I

The points labeled "normal" in Figure 5.11.4 give our best estimate of the total radiation absorbed in the lead glass. Interactions in the regenerator are the main source for the neutron beam. When the regenerator and shadow absorber materials are both changed to vacuum, the radiation decreases by about 50% at the center and from a factor of two beyond 20 centimeters to an order of magnitude at the edges. The regenerator is comparatively less significant for the K_L beam. All decays were turned off for the run labeled "no decays" in Figure 5.11.4a. The difference between these points and the "normal" points marks a level which cannot be reduced. Since the points fall by a factor of 5 everywhere, decays must account for ~80% of the damage due to the K_L beam. Both the regenerator and the TC's were simulated for the "no decays" run.

The TC material (2 cm of scintillator plus wrapping plus air) is a source of damage mainly inside a 40 centimeter radius. For neutrons the TC's were the source of 1/3 to 1/2 the damage. For K_L , they did not contribute significantly compared to the other sources.

Under the assumption that a week of running contains 10^4 pulses at the Tevatron, the points can be converted to rads/week. Figure 5.11.5 has the Monte Carlo results for several assumptions on the n/K_L ratio. The pair of curves for each condition represents the statistical difference in two different runs. Figure 5.11.6 has the prediction superimposed on the data, and the agreement is reasonable using the $n/K_L = 2$ (for the E731 vacuum beam); the value that best matches other data from E731 as discussed in section 5.2.

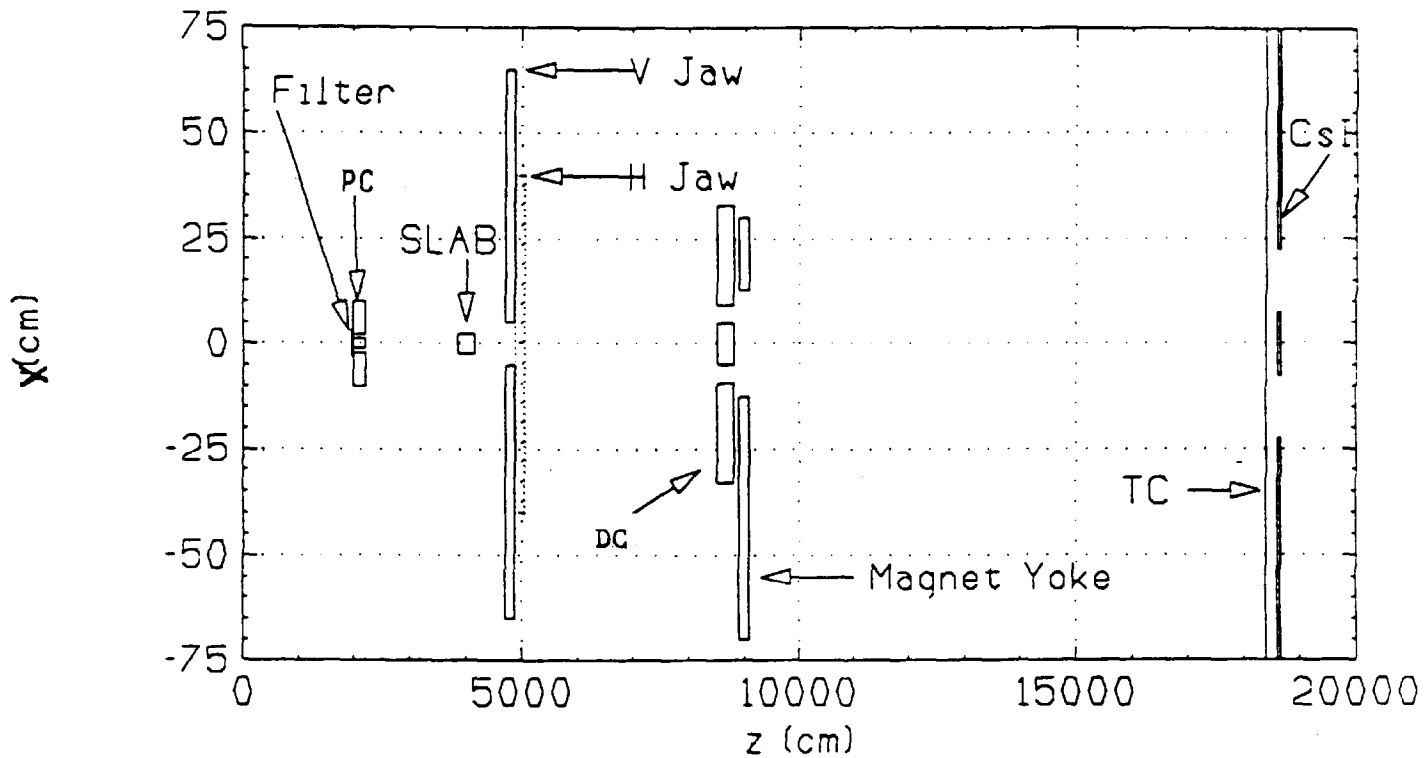
Findings

Given the overall good fits to E731 and E799-I for the simulation model, we believe that the main sources of damage are identified. In E731, background from both K_L and neutron interactions in the regenerator dominates everywhere except within the blocks between the beams. Even there it contributes approximately 20% of the damage. These statements are based on Figures 5.11.4. The TC's explain about half the damage from neutrons near the center, but much less for $r > 40$ cm. A high energy neutron interaction in scintillator can make up to 50 secondary particles, mostly pions, that do not deposit a lot of energy in the thin TC's, but which are largely absorbed in the calorimeter that follows within ≈ 2 meters. For K_L , the counters were not a major contributor because K_L decays are a more prolific source. Much of our confidence in this simulation is due to the fact that it not only gets about the right magnitude of the damage for both E731 and E799 but also reproduces the observation that the lead glass radiation damage falls off with increasing radius much more steeply when the regenerator is absent.

5.11.2 Projections for KTeV—E799II and E832

In KTeV, the neutral beam will be more effectively collimated than in the earlier experiments. Figure 5.11.12 shows the plan and elevation views.

(a) Plan View



(b) Elevation View

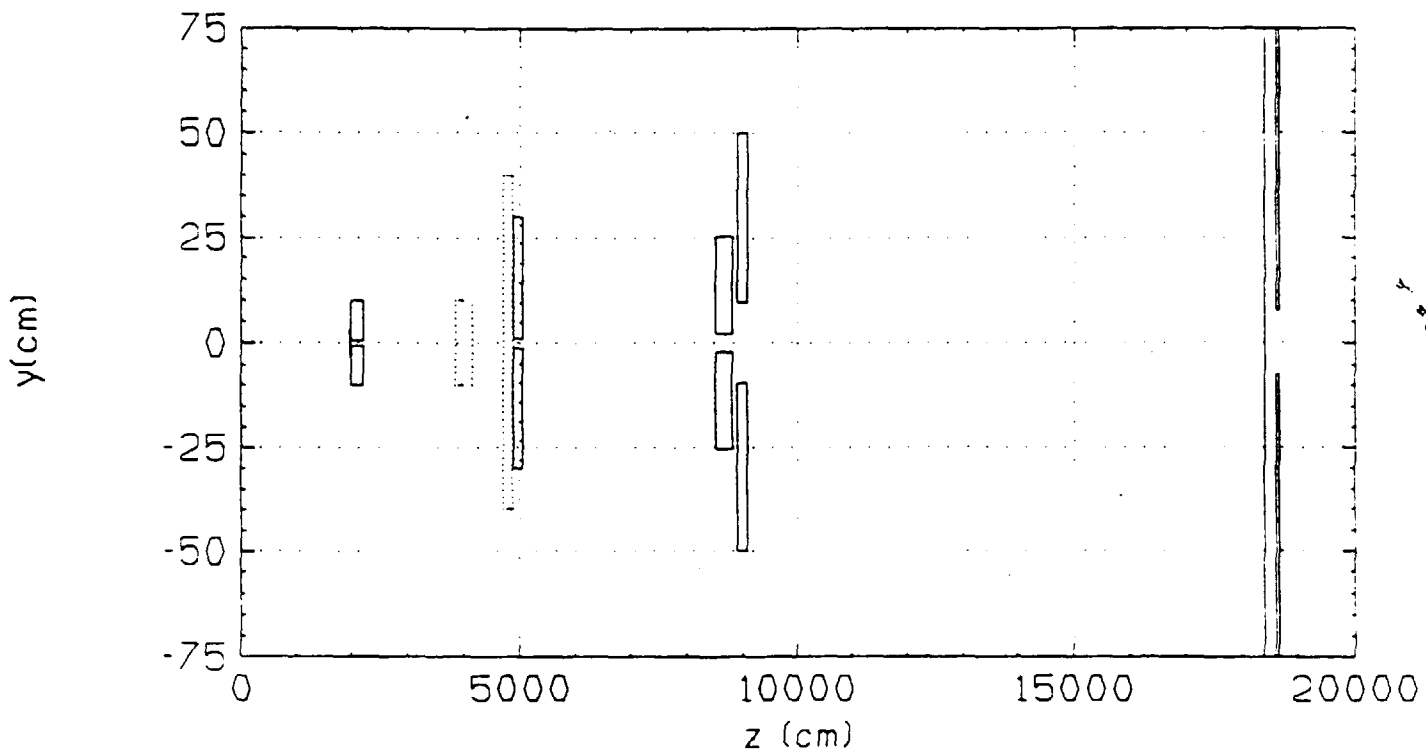


Fig. 5.11.12 KTeV Beam

E799-II

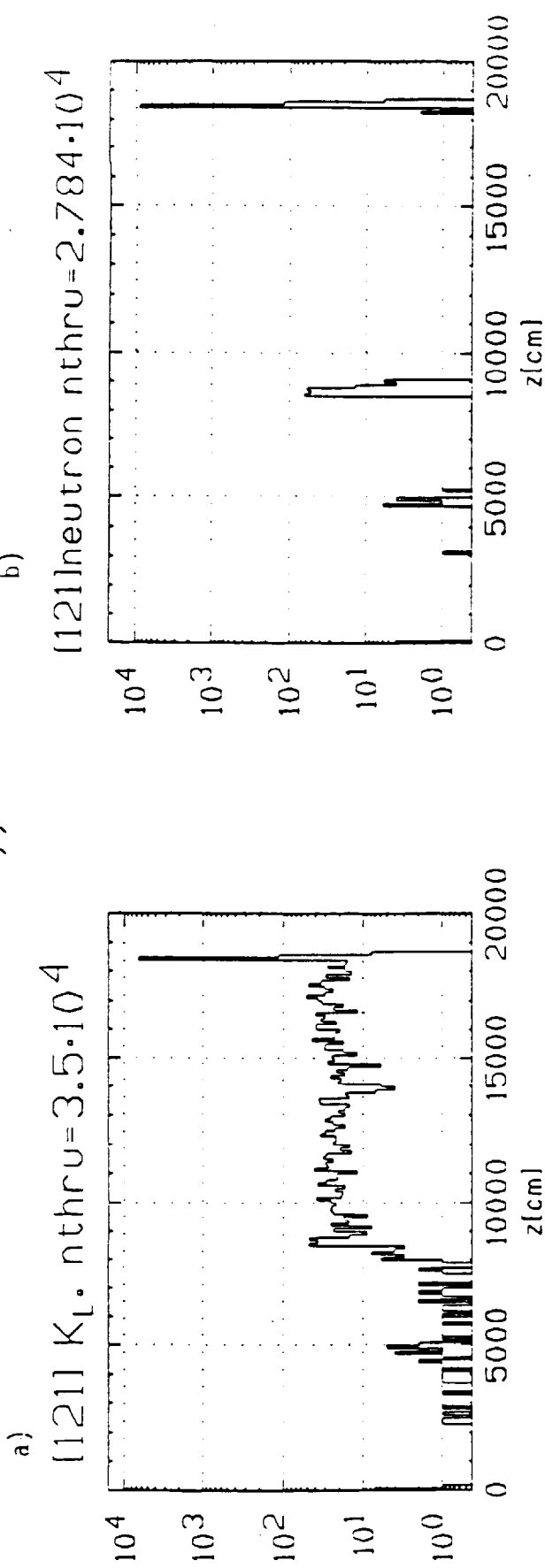
The K_L flux will be 2.9×10^8 for the sum of two beams. The elements in the E799-II simulation are:

- 1.) Pb filter
- 2.) Cu primary two-hole collimator (PC)
- 3.) Fe vertical slab separating the beams horizontally
- 4.) Fe x-defining vertical jaws
- 5.) Fe y-defining horizontal jaws
- 6.) Sweeping magnet from 23-29 m, 25 kg, 40cm(x), 4cm(y)
- 7.) Cu downstream two-hole collimator (DC)
- 8.) DC Insert
- 9.) Sweeping magnet
- 10.) Trigger counters (TC)
- 11.) CsI calorimeter

Material in the vacuum window, helium, and drift chambers was included. Figure 5.11.13 shows the origins of CsI hits. Four cases are shown: n and K_L with and without TC beamholes. Each run gave approximately 3×10^4 beam particles through the CsI holes. The individual numbers (n_{thru}) are printed on the plots. Compared with the expected flux of 2.9×10^8 this tiny sampling (6×10^5) is a potential weakness of the Monte Carlo. It is possible that tails of distributions unsampled in this simulation could change the picture.

The z-coordinate of the vertex of any particle entering the CsI is enough to identify where the background comes from. K_L 's decay over the whole path from 80 to 200 meters so the distribution is continuous from the downstream collimator to the CsI with a spike at the TC plane. The runs with TC beamholes show smaller spikes at the TC where some of the kaon daughters interact. (The main beams of course pass through.) A few cases where neutrons lead to CsI hits nearly all originate in the DC at $z \approx 88$ meters. Figure 5.11.13a(b) shows $K_L(n)$ if the TC's are solid across the beam, and Figure 5.11.13c(d) if the TC's have beamholes. CsI hits go up a factor of ≈ 25 ($7000/300$, from the Figure 5.11.13a,c spike at $z \approx 186$ meters) due to particles starting at the trigger plane.

Solid Trigger Counters^{b)}



Trigger Counters with Beam Holes

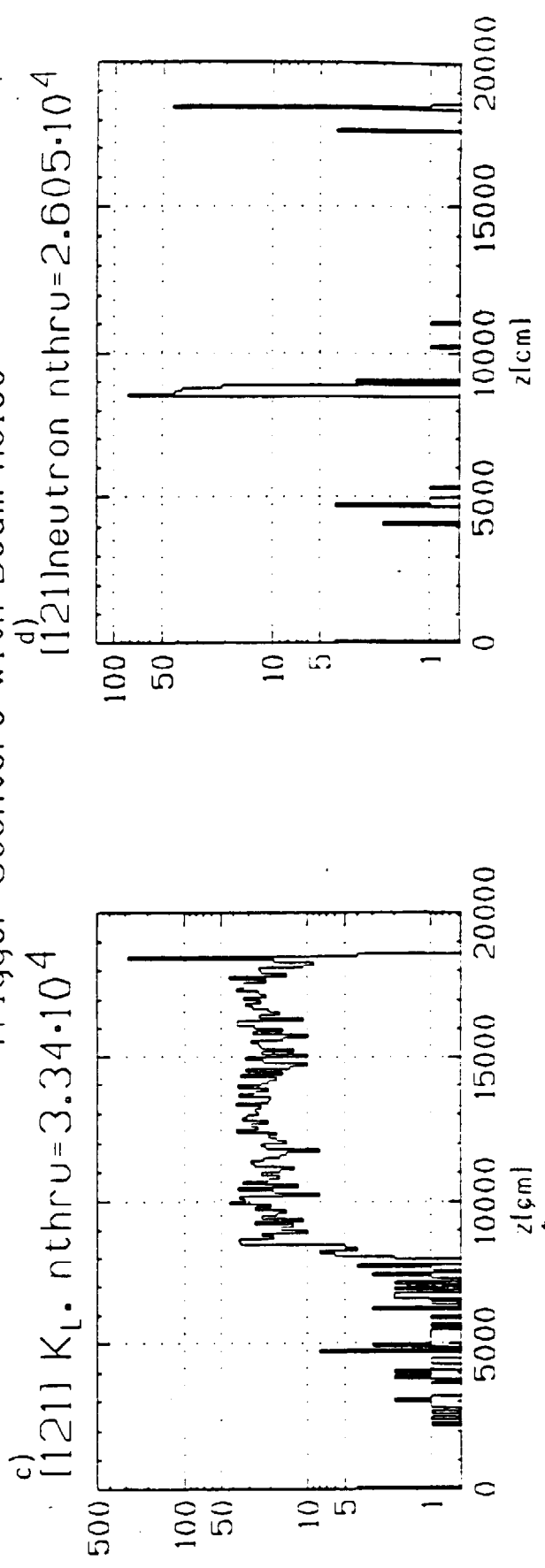


Fig. 5.11.13 $\vec{E}799$ -II Sources of CsI Hits

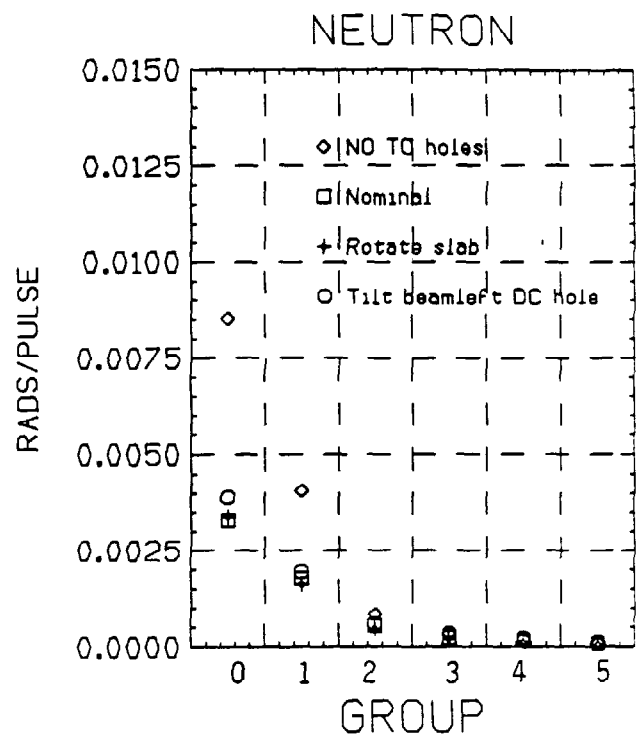
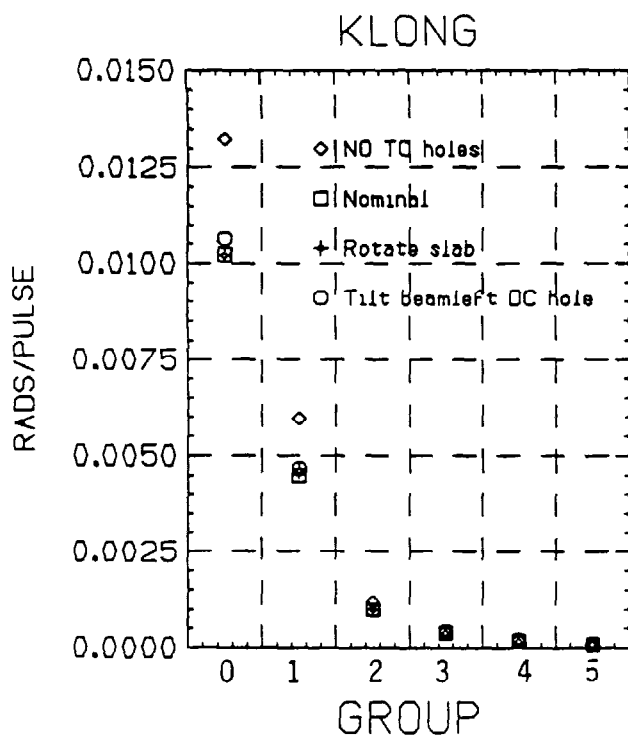
To cite numbers for radiation damage as a function of position, the calorimeter is divided into square cells of width 15 cm. The numeration is shown in table below. The energy deposits in the CsI are plotted in Figure 5.11.14a (b) for K_L (neutrons). The damage from the kaons is not increased much above that from decays by the TC material. However, damage from neutrons in the pulse goes from negligible to near equality with the K_L including the TC material. Also shown are the effects of rotating the slab collimator by 2 mrad creating a horizontal tilt and of rotating the DC 2 mrad to create a vertical tilt. Even though this 2 mrad rotation is more than an order of magnitude larger than expected alignment tolerances, the radiation damage does not significantly increase.

Table of numbering of CsI Cells

5	5	5	5	5	5	5	5	5	5	5	5	5
5	4	4	4	4	4	4	4	4	4	4	4	5
5	4	3	3	3	3	3	3	3	3	3	4	5
5	4	3	2	2	2	2	2	2	2	3	4	5
5	4	3	2	1	1	1	1	1	2	3	4	5
5	4	3	2	1		0		1	2	3	4	5
5	4	3	2	1	1	1	1	1	2	3	4	5
5	4	3	2	2	2	2	2	2	2	3	4	5
5	4	3	3	3	3	3	3	3	3	3	4	5
5	4	4	4	4	4	4	4	4	4	4	4	5
5	5	5	5	5	5	5	5	5	5	5	5	5

How serious this TC material is depends on the n/K ratio. Figure 5.11.14c predicts 500 rads/week for a worst case. This damage would be less by a factor of two if the neutral beam can pass through holes in the TC. Repeating this analysis for the double solid angle option (.50 mster.), gives radiation damage which increases only slightly more than for the kaon flux. This work will be documented in a future KTeV memo.

The predicted beam profiles at the CsI for the case with TC beamholes are shown in Figure 5.11.15.



EFFECT OF TRIGGER COUNTER MATERIAL

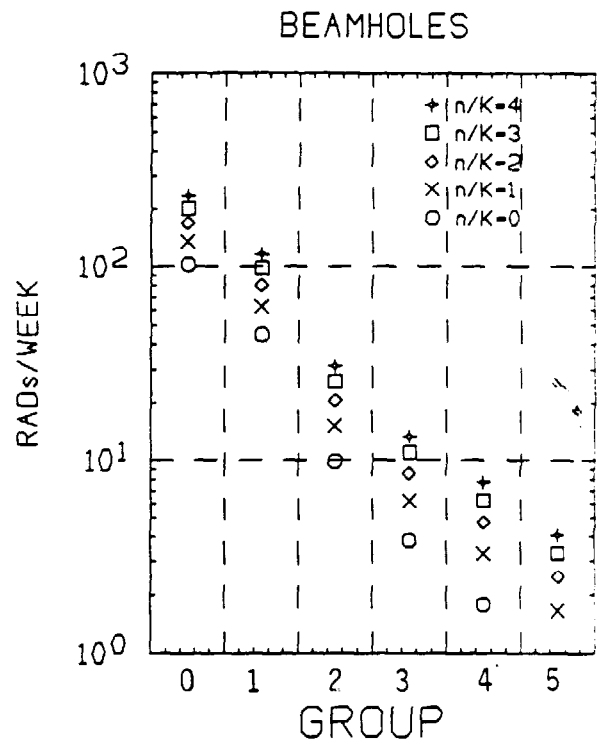
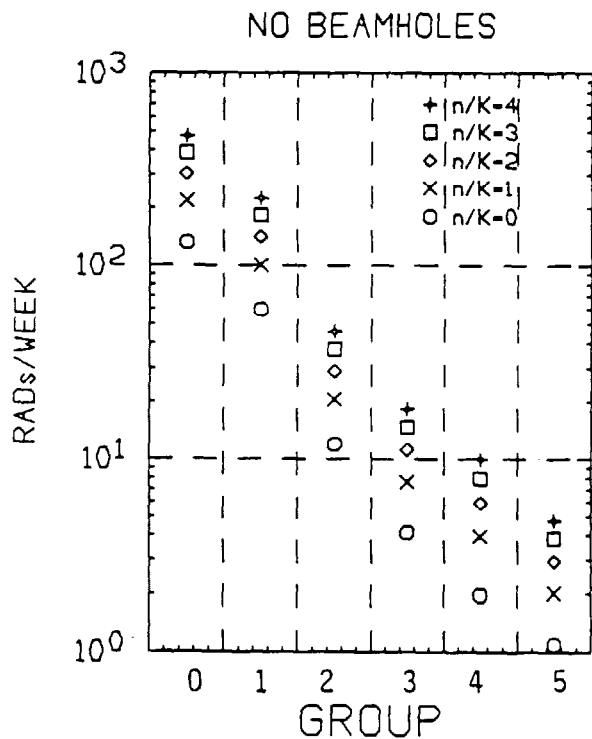
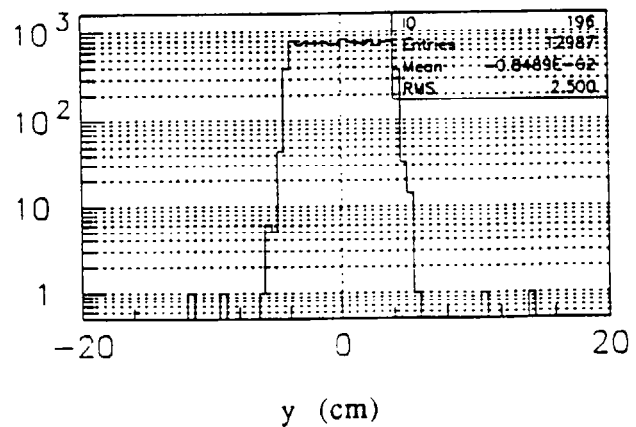
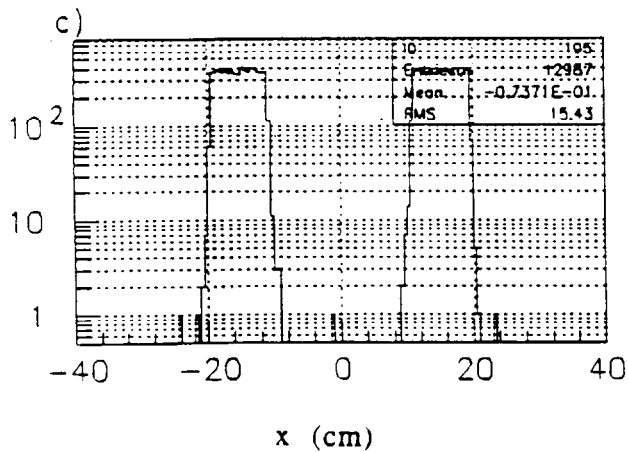
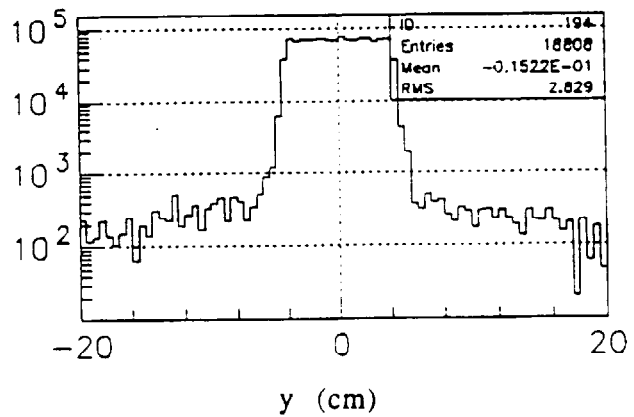
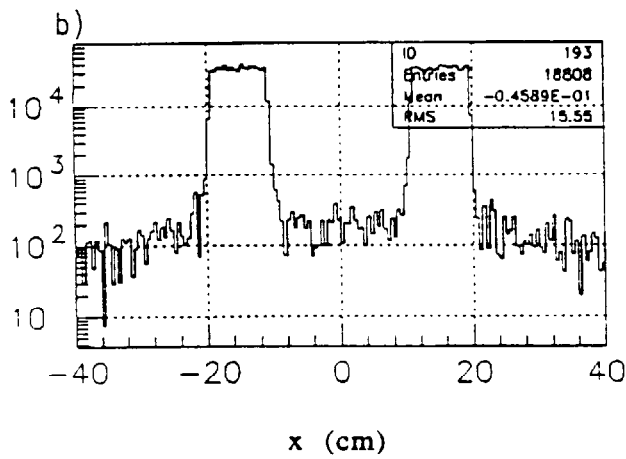
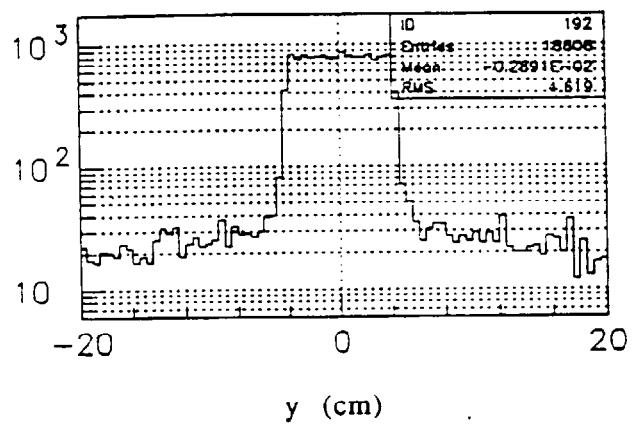
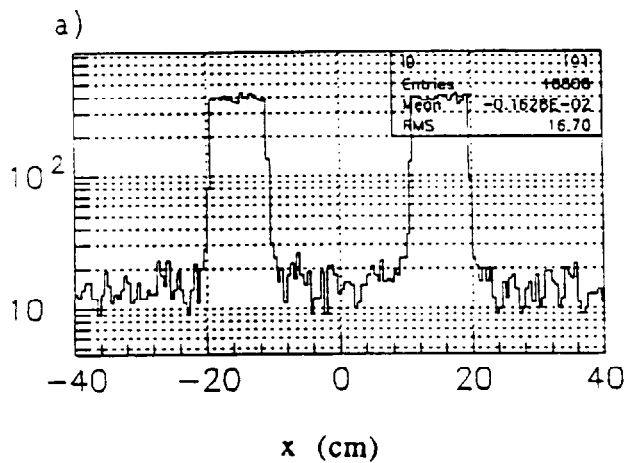


Figure 5.11.14. E799-II Radiation damage vs CsI group

Fig. 5.11.15 a) The flux of all particles hitting a plane just of the CsI predicted for E799II.
 b) The flux weighted by particle energy.
 c) The flux of KL's.



E832

In addition to the beam elements listed above, E832 adds:

- 13.) Be shadow absorber
- 14.) Regenerator

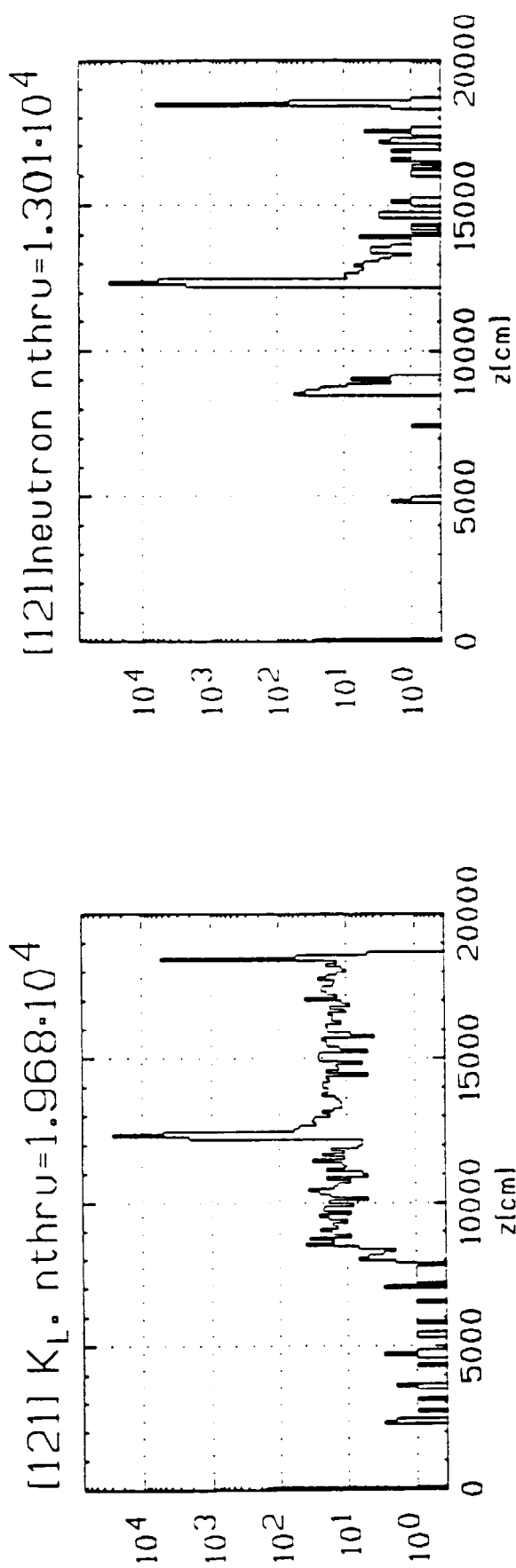
The K_L flux for E832 will be about 3.5×10^7 for the vacuum beam. The CsI background picture is different from that of E799II. The regenerator dominates; Figure 5.11.16 shows the z-origin of particles that enter the front face of the CsI; the regenerator at 120 meters is prominent, especially in the neutron runs. Figure 5.11.17 summarizes the energy dumped in the CsI. The TC damage adds about 25% to that from the regenerator for both n and K_L . The beam profiles are shown in Figure 5.11.18 for the case with TC beamholes.

Conclusion

The main features of radial dependence of measured radiation damage to the lead glass calorimeter in E731 and E799 are reproduced with a GEANT simulation. The level of damage is reproduced to a factor closer to two, and the shape is better than that. The contrast between E731 and E799 and the r-dependence is reproduced. A simulation to predict damage in CsI gives a level that almost surely will approach 200-300 rads/week at the center of the calorimeter in E799-II. The level may go as high as 500 rads/week depending on the neutron to kaon ratio of the beam. The damage will be reduced by about a factor of two by having holes in the trigger counters. In E832, regenerator-induced background is so high that the trigger counter material is almost of no incremental effect. Studies of the acceptance for $K_L \rightarrow p^+ p^-$ with beam holes in the trigger counters⁵¹ indicate a small loss in acceptance. Therefore, we plan to run both E832 and E799II with the same trigger hodoscope which has beam holes.

⁵¹ Belz, J., et al., KTeV 0200, Modified KTeV Trigger Bank Layout, 5/5/94.

Solid Trigger Counters



Trigger Counters with Beam Holes

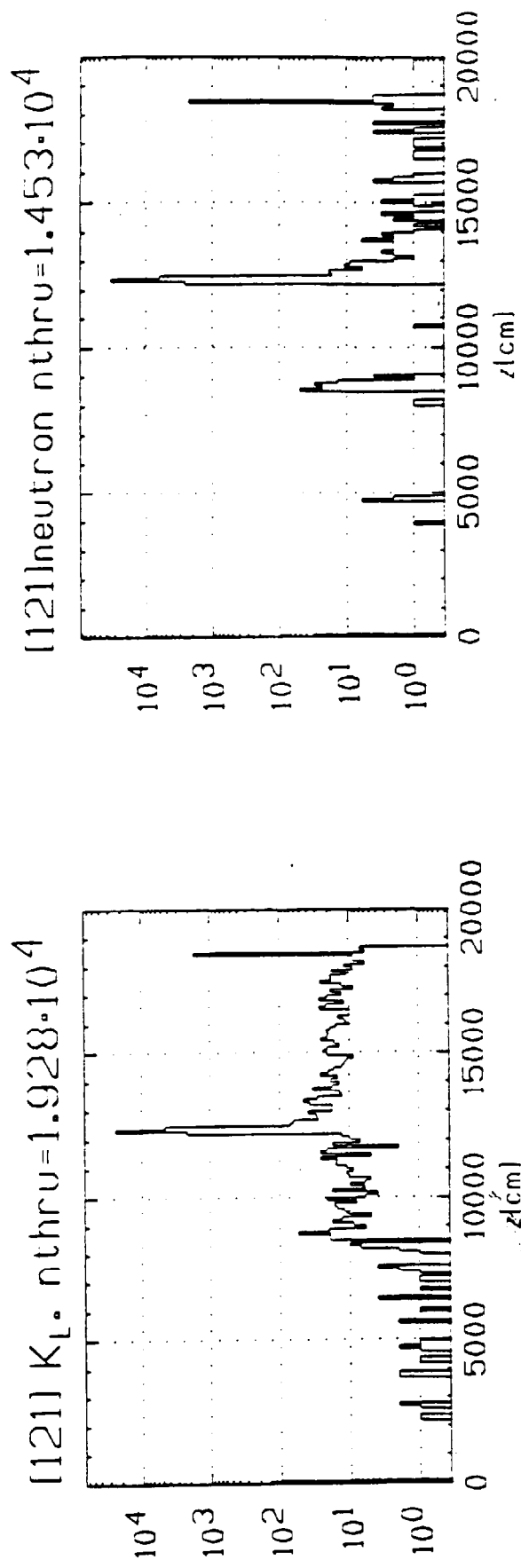
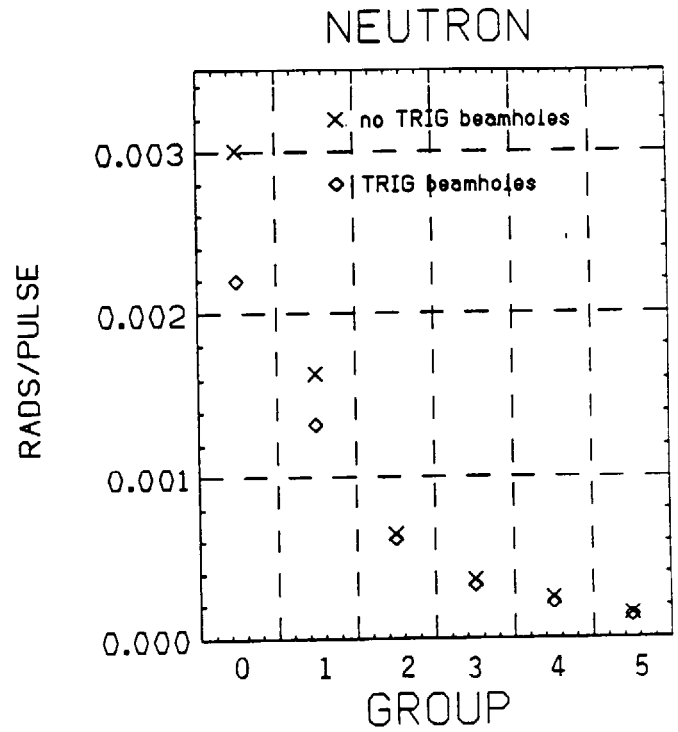
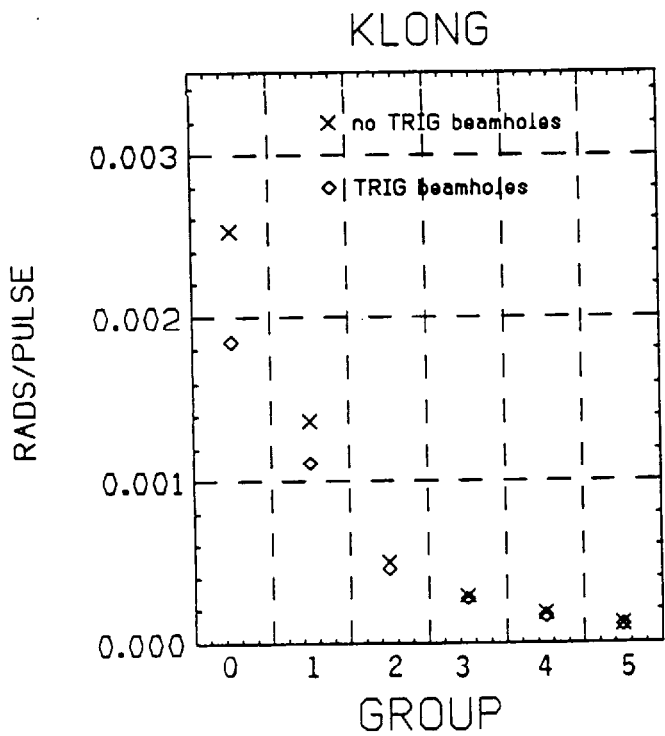


Fig. 5.11.16 E832 Sources of CsI Hits



EFFECT OF TRIGGER COUNTER MATERIAL

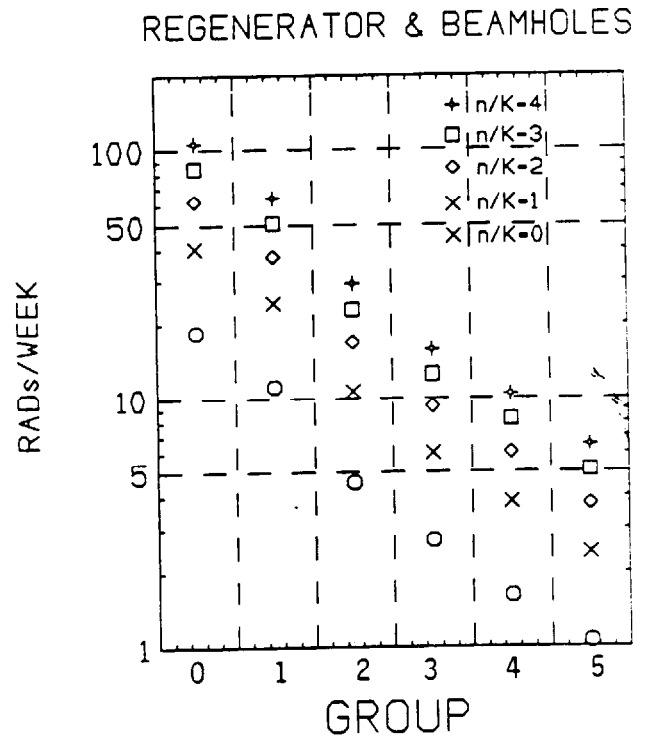
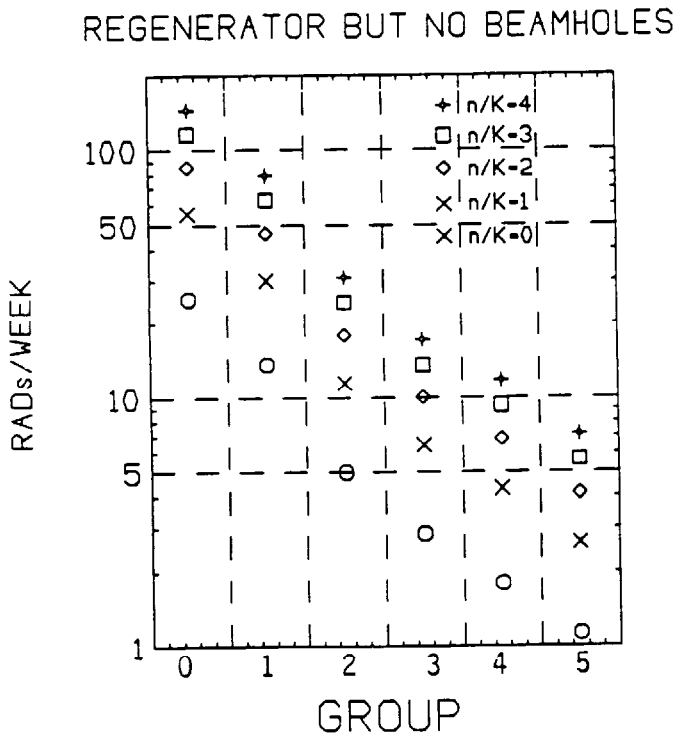


Figure 5.11.17 E832 Radiation damage vs CsI group

Fig. 5.11.18 a) The flux of all particles hitting a plane the CsI for E832 (showing both vacuum and regenerator beams).
 b) The flux weighted by particle energy.
 c) The flux of K_L 's.

